Energy Conversion and Management 359 (2026) 121511

Contents lists available at ScienceDirect

Energy Conversion and Management

journal homepage: www.elsevier.com/locate/enconman

Research Paper

Optimizing Algeria's solar potential: end-to-end PV siting, performance mapping, and techno-economic insights

Mawloud Guermoui [a,b,*], Abdelfetah Belaid [b], Abdelkader Riche [c], Farid Melgani [a]

[a] Department of Information Engineering and Computer Science, University of Trento, Trento, Italy
[b] Unité de Recherche Appliquée en Energies Renouvelables, URAER, Centre de Développement des Energies Renouvelables, CDER, Ghardaïa, Algeria
[c] Department of Earth Sciences, University of Florence, Florence, Italy

ARTICLE INFO

Keywords:
Site selection
Multi-criteria analysis
PV plant
Economic study
PV atlas

ABSTRACT

Large-scale photovoltaic (PV) deployment in Algeria requires robust and transparent siting and planning methods that jointly account for solar resource quality, infrastructure accessibility, environmental safeguards, and power-system constraints. This study develops a nation-scale, high-resolution (100 m) PV site-selection and planning framework to support evidence-based investment and strategic grid expansion under Algeria's pronounced north–south mismatch between optimal solar resources in the Sahara and major demand centers in the North. A comprehensive geospatial database of PV performance and siting drivers was harmonized from authoritative sources and integrated into a transparent GIS-MCDA workflow using explicit exclusion masks and fuzzy AHP (FAHP) expert weighting. Suitability maps were produced for (i) utility-scale PV hubs and (ii) low-/distributed PV, while an additional offline scenario, removing proximity-to-grid and road constraints, was introduced to identify intrinsically favorable but currently remote opportunities. PV performance was quantified through a production atlas comparing horizontal and optimally tilted systems using temperature-corrected plane-of-array irradiance, yielding annual alternating-current (AC) energy potentials of 242–309 GWh·km^{-2}·yr^{-1}. Conceptual north–south interconnection corridors were evaluated to improve access to high-quality clusters under realistic land and environmental constraints. A techno-economic assessment mapped site-specific levelized cost of electricity (LCOE) of 3.63–4.63 cEUR·kWh^{-1}, including connection and access cost adders, while a screening-level environmental and CO_2 analysis estimated avoided emissions of 67.91–86.65 kt CO_2·km^{-2}·yr^{-1} under a gas-displacement baseline. Robustness was further examined through Monte Carlo uncertainty and targeted sensitivity analyses. Under the grid-connected scenario, the minimum median LCOE reached 3.91 cEUR·kWh^{-1}, while a representative low-LCOE tilted-PV site showed a wider LCOE range of 1.4–7.27 cEUR·kWh^{-1} under varying economic assumptions. Compared with prior Algerian studies, the framework expands deployment scales, strengthens the constraint stack, and adds actionable grid-scenario, uncertainty, and portfolio-sizing analyses for strategic PV planning.

1. Introduction

Global energy demand has risen consistently over recent decades. In 2024, it grew by 2.2% to nearly 650 EJ [1]. Fossil fuels still dominate the mix around 80% of global primary energy in recent years with only a gradual decline under current policies [2,3]. This dependence carries environmental and safety risks, including SO_x, NO_x, and other greenhouse-gas emissions; energy-related CO_2 emissions rose 0.8% in 2024 to 37.8 Gt [4]. Large-scale decarbonization of fossil fuels via post-combustion capture remains limited and often costly, with deployment expanding only modestly and capture costs high for dilute streams [5,6]. Consequently, accelerating renewables and other low-carbon options together with efficiency remains the most practical pathway for sustainable energy development [1].

To satisfy rising electricity demand while cutting emissions, solar photovoltaics has become a pivotal option: in 2024 the global weighted-average LCOE for utility-scale PV ≈ USD 0.043/kWh, and >90% of new renewable capacity undercut fossil-fired alternatives [7]. This cost and manufacturability profile enables rapid scale-up provided projects are sited where resource, grid access, and environmental constraints align. Yet PV is inherently spatial: irradiance regime, atmospheric conditions, temperature, terrain, land use, and infrastructure proximity jointly determine both energy yield and feasibility. Credible planning therefore

* Corresponding author at: Department of Information Engineering and Computer Science, University of Trento, Trento, Italy.
E-mail address: mawloud.guermoui@unitn.it (M. Guermoui).

https://doi.org/10.1016/j.enconman.2026.121511
Received 1 January 2026; Received in revised form 14 April 2026; Accepted 14 April 2026
Available online 29 April 2026

Nomenclature

Acronyms

ABC Artificial Bee Colony (optimization algorithm)
AC Alternating current
AHP Analytic Hierarchy Process
AHP-DEA AHP + Data Envelopment Analysis
AHP-MCDM AHP-based Multi-Criteria Decision Making
AHP-OH Optimized-Hierarchy AHP
AHP-PROMETHEE AHP + PROMETHEE method
AHP-TOPSIS AHP + TOPSIS method
AHP-WLC AHP + Weighted Linear Combination
ANP Analytic Network Process
AUC Area Under the Curve (ROC–AUC)
AVHRR Advanced Very High Resolution Radiometer
BWM Best–Worst Method
CA Classification Accuracy (overall accuracy)
CAPEX Capital expenditure
CCUS Carbon Capture, Utilization and Storage
CF Capacity factor
CI Consistency Index
CM SAF EUMETSAT Satellite Application Facility on Climate Monitoring
CO_2 Carbon dioxide
COP Conference of the Parties (UN climate process)
CR Consistency Ratio
DC Direct current
DEM Digital Elevation Model
DHI Diffuse Horizontal Irradiance
DNI Direct Normal Irradiance
ESA European Space Agency
ES Extremely suitable (suitability class)
ESMAP Energy Sector Management Assistance Program
EU European Union
EUMETSAT European Organisation for the Exploitation of Meteorological Satellites
EUR Euro
FAHP Fuzzy Analytic Hierarchy Process
FAHP-GIS FAHP integrated with GIS
FF-SWARA Fermatean Fuzzy Step-wise Weight Assessment Ratio Analysis
FT-Transformer Feature Tokenizer Transformer (tabular deep-learning model)
GDAL Geospatial Data Abstraction Library
GHI Global Horizontal Irradiance
GIS Geographic Information System
GRASS Geographic Resources Analysis Support System
GTI Global Tilted Irradiance
GW Gigawatt
GWh Gigawatt-hour
HV High voltage
IEA International Energy Agency
IRENA International Renewable Energy Agency
LCOE Levelized Cost of Electricity
LCPM Least-Cost Path Model
LS Low suitable
LULC Land Use / Land Cover
MAUT Multi-Attribute Utility Theory
MCDA Multi-Criteria Decision Analysis
MCDM Multi-Criteria Decision Making
ML Machine Learning
MLP Multi-Layer Perceptron
MSCA Marie Skłodowska-Curie Actions
MVIRI Meteosat Visible and InfraRed Imager
MW Megawatt
MWh Megawatt-hour
N-S North–South
NASA National Aeronautics and Space Administration
ND No-deployment zone (class)
NDVI Normalized Difference Vegetation Index
NREL National Renewable Energy Laboratory
O&M Operation and maintenance
OPEX Operating expenditure
PM2.5 Particulate matter with aerodynamic diameter $\leq$ 2.5 μm
POWER Prediction Of Worldwide Energy Resources (NASA POWER)
PS Poorly suitable
PV Photovoltaic
PV-DGs Photovoltaic distributed generators
PVOUT PV power output
PVPPs Photovoltaic power plants
QGIS QGIS (open-source GIS software; historically “Quantum GIS”)
RF Random Forest
RI Random Index (AHP consistency reference)
SAGA System for Automated Geoscientific Analyses (GIS software)
SAPM Sandia Photovoltaic Array Performance Model
SARAH Surface Solar Radiation Data Set – Heliosat
SCF Solar Capacity Factor (as written in your tables)
SDU Sunshine duration
SEVIRI Spinning Enhanced Visible and InfraRed Imager
SHAP SHapley Additive exPlanations
SNASPE National system of protected areas
SO_2 Sulfur dioxide
SONELGAZ Algeria’s national electricity and gas utility
SR Solar radiation
SRTM Shuttle Radar Topography Mission
STC Standard Test Conditions
TFN Triangular Fuzzy Number
TFNs Triangular Fuzzy Numbers
TFT Triangular-Fuzzy TOPSIS
TL Linke turbidity factor
TOPSIS Technique for Order Preference by Similarity to Ideal Solution
TWh Terawatt-hour
UNESCO United Nations Educational, Scientific and Cultural Organization
USD United States dollar
VAT Value Added Tax
VS Very suitable
WACC Weighted Average Cost of Capital
WDPA World Database on Protected Areas
WHS World Heritage Site(s)
WLC Weighted Linear Combination
WLC-ACM Weighted Linear Combination with Area Constraint Method
WMO World Meteorological Organization
WMR Western Mediterranean Region
WSM Weighted Sum Method
XGBoost eXtreme Gradient Boost

moves from global targets to site-specific evidence combining climatological irradiance (horizontal and optimally tilted), temperature-corrected plane-of-array modeling, and a transparent geospatial site-selection procedure with explicit exclusions, documented weights, and sensitivity checks.

Translating PV's cost advantage into dependable supply requires defensible site-suitability analysis framed as a multi-criteria decision. Site selection is foundational to project feasibility. Accordingly, GIS-based spatial analysis is used to screen and prioritize candidate locations. This analysis integrates climatological drivers (irradiance regime and stability, operating temperature), environmental and planning constraints (land cover/use, protected areas, terrain, settlement and buffer exclusions), and infrastructure/access factors (proximity to transmission and distribution grids, substations, and roads).

Over the past two decades, the combination of GIS and multi-criteria methods widely referred to as GIS-MCDA has gained prominence in energy planning and policy evaluation, including solar, biomass, wind, and storage siting applications [8]. Comprehensive reviews catalog site-suitability methods, decision criteria and restrictions, and tool choices in GIS environments; notably, over 80% of studies address grid-connected PV, with Analytic Hierarchy Process (AHP) the most common approach to derive weights [9]. Method families used in GIS-MCDA include TOPSIS, ELECTRE [10], Weighted Linear Combination (WLC), AHP/ANP, and various hybrids, with WLC frequently adopted for relative suitability scoring [11,12]. Selecting the most determinative criteria remains critical, and the literature notes that social and risk dimensions are often underrepresented despite their importance for permitting and bankability. Beyond resource quality, recent workflows also overlay suitability with demand/hosting proxies (e.g., spatial load allocation) to align generation potential with grid absorption and near-term deliverability.

To position the present study within established PV siting practice, the following state-of-the-art synthesis summarizes recent GIS–MCDA contributions and their evolution toward decision-relevant planning.

1.1. State of the art

GIS-based multi-criteria decision analysis (GIS–MCDA) is widely adopted for PV siting, integrating solar-resource indicators, terrain constraints, land-use/land-cover screening, and proximity-to-infrastructure factors to derive suitability classes. Prior studies differ in spatial scale, criteria design, weighting/aggregation methods, and the extent to which performance, techno-economic, and environmental dimensions are integrated. The following paragraphs provide a study-by-study narrative synthesis of representative contributions. Doorga et al. [12] proposed a GIS-based MCDA framework for solar farm siting in Mauritius, demonstrating practical suitability mapping at island scale; however, the results remain largely score-based and are not coupled to a PV production atlas or scenario-based grid accessibility assessment. Zambrano-Asanza et al. [8] developed a GIS-based multi-criteria site selection approach for PV power plants in Ecuador, explicitly integrating spatial overlay with electric load information; nevertheless, the methodology remains focused on suitability ranking without explicit PV yield modelling and without grid expansion scenarios. Imam et al. [13] assessed land suitability and techno-socio-economic feasibility for solar PV and wind development in Saudi Arabia, including variability considerations; yet, a unified workflow linking performance-based PV production mapping with grid-pathway scenarios and fully transparent environmental screening is not systematically established. Halimi et al. [14] presented a spatially optimized PV site selection framework in Algeria using high-resolution data, GIS, and multicriteria analysis; however, the study does not explicitly deliver a PV production atlas nor test alternative grid-access pathways via scenarios, limiting its suitability-to-feasibility translation. Díaz-Cuevas et al. [15] provided renewable energy planning and mapping in Algeria within a national planning perspective; still, the siting outputs remain primarily suitability-driven without performance-based production mapping and without scenario-based grid accessibility analysis. Wang et al. [16] investigated suitable large-scale solar farm locations in China's desert regions while incorporating environmental considerations; however, the decision chain remains challenging to benchmark economically because key LCOE inputs are not consistently reported. Hamad et al. [17] combined solar resource mapping, site suitability, and techno-economic feasibility analysis for utility-scale PV plants in Afghanistan. This represents one of the few studies that moves beyond suitability-only outputs. However, techno-economic transparency remains uneven, particularly for degradation, cost boundaries, and financing assumptions, and grid access is not addressed through planning scenarios.

Nafi'shehab et al. [18] performed a multi-technique comparative MCDM analysis for identifying optimal solar farm locations, highlighting sensitivity to methodological choices; however, without performance-based PV yield modelling and without grid development scenarios, the resulting "optimality" remains primarily criteria-dependent rather than feasibility-grounded. Rekik and El Alimi [19] developed a GIS-based MCDM modelling approach for evaluating large-scale solar PV installation in Tunisia; yet, the outcome remains relative suitability without explicit PV yield modelling and without scenario-based infrastructure planning. Al-Awadhi et al. [20] applied a GIS-based AHP suitability framework for solar farms in Al Duqm, Oman; still, feasibility remains limited by the absence of PV production atlas modelling and the lack of scenario-based grid accessibility assessment. Elkadeem et al. [21] developed a spatio-temporal decision-making model for utility-scale solar PV, onshore wind, and hybrid PV/WT deployment in Saudi Arabia. The framework integrates ERA5 reanalysis, multi-criteria spatial screening of more than twenty constraint/evaluation criteria, energetic-complementarity analysis, and a techno-economic assessment that includes infrastructure-cost components and LCOE ranges. The study provides national-scale priority zones and land-allocation guidance toward Saudi Vision 2030 targets, while grid availability is treated primarily through spatial accessibility/cost factors rather than scenario-based transmission-corridor planning. Demir et al. [22] introduced a novel procedure for the AHP method for solar PV farm site selection, improving methodological rigor; yet, without performance-based PV production mapping and grid scenarios, suitability remains a relative ranking. Zhao et al. [23] proposed a GIS-based and advanced MCDM framework for siting wind–PV complemented storage power plants in China, incorporating inter-criteria correlation and interactive decision making; however, the study does not explicitly present a PV production atlas nor grid-development scenarios that would support feasibility-ranked planning. Zhang and Zhao [24] developed a hybrid MCDM approach for PV power plant siting based on matching resource–demand quantity and quality, improving demand-aware screening; nevertheless, the workflow does not explicitly translate suitability into performance-based PV production mapping or scenario-driven grid access. Farfán et al. [25] assessed socio-environmental and technical factors for PV-based hydrogen production in Antofagasta, Chile, expanding the siting scope toward sector coupling; still, PV production atlas modelling and grid corridor scenarios are not systematically integrated into a feasibility-ranked pipeline. Saraswat et al. [26] analyzed multi-renewable energy potential sites in India using GIS and hybrid MCDM and reported LCOE-related outcomes; however, incomplete disclosure of harmonized assumptions limits reproducibility and comparability. Flora [27] applied a GIS-based Monte Carlo and MCDM approach for site suitability analysis of solar-hydrogen production in Cameroon, strengthening uncertainty awareness; yet, PV production atlas modelling and grid-access scenarios are not systematically operationalized. Li et al. [28] proposed a three-stage framework to support large-scale PV solar farm site selection in China, strengthening process structure; still, decision outputs remain mainly suitability-focused without explicit performance-based PV production mapping and grid scenario pathways. Santana-Sarmiento and Velázquez-Medina [29] proposed a GIS-based method to assess renewable energy self-consumption capacity in Spain and reported LCOE-related results; however, degradation is not reported in the extracted LCOE summary and cross-study comparability remains limited by heterogeneity of economic definitions. Metegam et al. [30] evaluated on-grid and off-grid PV sites in Cameroon using GIS, fuzzy logic, and multicriteria analysis; nevertheless, the analysis does not explicitly deliver a PV production atlas and does not explore grid access through development scenarios. Yilmaz et al. [31] applied GIS and fuzzy AHP for solar power plant site selection in the Western Mediterranean region of Türkiye; however, the approach remains suitability-focused without explicit PV yield modelling and without scenario-driven grid access. Xiao et al. [32] evaluated land reuse for carbon mitigation through PV deployment in China's open-pit mining areas, strengthening land-reuse framing and decarbonization relevance; still, PV production atlases and grid corridor scenarios are not presented as an integrated feasibility workflow. Richards et al. [33] developed a multi-criteria site suitability approach linked to greenhouse gas emission reduction for sustainable solar deployment; however, suitability is not consistently linked to performance-based PV yield modelling nor scenario-based grid planning. Elkadeem et al. [34] developed a GIS-MCDM geospatial decision-making model for Egypt to map 1 km^2 suitability and geographical-technical–economic potential for solar PV and onshore wind. The study used 16 criteria and reported associated energy potential and average LCOE estimates (≈57.84 $/MWh for PV and ≈32.36 $/MWh for WT). However, the framework is oriented toward multi-technology potential zoning. It does not explicitly incorporate PV-specific production-atlas modelling, scenario-based transmission-corridor planning, or systematic sensitivity testing.

Okazawa et al. [35] investigated PV power plant installation constraints in the Tokyo metropolitan area, Japan, emphasizing land use and regulatory ordinances; yet, PV production atlas modelling and grid scenarios are not central to the framework. Vasudevan et al. [36] assessed GIS-based PV farm suitability using a multi-criteria approach in Southern Tamilnadu, India; however, results remain relative suitability without PV yield modelling and without scenario-based grid accessibility. Li et al. [37] proposed an interaction model to optimize PV farm location in China, strengthening representation of interactions among siting factors; still, feasibility remains limited without a PV production atlas and without infrastructure pathway scenarios. Boube et al. [38] conducted a geospatial evaluation of solar potential for hydrogen production site suitability across Niger using a GIS–MCDA approach for off-grid and utility-scale systems and reported LCOE-related values; nevertheless, key LCOE assumptions (notably degradation and WACC in the extracted summary) are not consistently reported, limiting comparability. Bawazir et al. [39] investigated optimum on-grid connected ground-mounted PV systems from a system-design perspective; however, the siting/planning dimension does not explicitly integrate PV production atlases and grid-development scenarios. Flora [40] performed an MCDM–GIS suitability analysis for PV integration and hydrogen co-production in Cameroon, strengthening sector coupling; still, PV production atlas and scenario-based grid-access planning are not consistently established. Ali et al. [41] assessed PV siting and CO_2 reduction through GIS-based spatial analysis in Jeddah, Saudi Arabia, strengthening mitigation framing; however, performance-based PV yield modelling and scenario grid planning remain limited. Fan et al. [42] assessed solar resource potential in the Western region of Jilin Province, China, using availability, stability, and concentration indicators, strengthening resource characterization; still, translating such indicators into performance-based PV production atlases and feasibility-ranked siting remains underdeveloped. Sharma and Sarin [43] evaluated solar site suitability using hybrid MCDM techniques in Punjab, India, strengthening methodological triangulation; nevertheless, PV production atlas modelling and grid-development scenarios are not included. Tang et al. [44] developed a policy-integrated multi-criteria spatial planning framework for PV siting in Liangshan Prefecture, China, strengthening policy alignment; however, PV production atlas and grid corridor scenario analysis are not fully integrated into feasibility ranking. Onuoha et al. [45] integrated GIS and AHP for PV farm site selection in Ikorodu, Nigeria, demonstrating applicability in rapidly urbanizing contexts; still, results remain relative suitability without PV yield modelling and without grid scenarios. Akay [46] investigated land suitability for PV farms and existing sites in Gaziantep, Türkiye, strengthening consistency checks against installed sites; however, PV production atlas and grid-access scenarios are not explicitly developed. Ashraf et al. [47] combined GIS and machine learning for PV site selection in Pakistan, strengthening data-driven screening; yet, feasibility still requires explicit PV yield modelling, grid pathway scenarios, and operational environmental screening. Shen et al. [48] published high spatial-resolution suitability layers to support feasible power plant siting in China, strengthening open spatial data support; nevertheless, suitability layers alone do not substitute for PV production atlases and scenario-driven grid feasibility. Lamien and Farzaneh [49] proposed an integrated land-use/land-cover–energy modelling framework for solar planning in future expansion areas in the Luxor region, Egypt, strengthening forward-looking land–energy integration; however, PV production atlas modelling and grid-access scenarios remain limited in many such workflows. Yang et al. [50] mapped development potential and priority zones for utility-scale PV on the Qinghai–Tibet Plateau, strengthening prioritization for challenging terrain; still, the link to performance-based PV yield and scenario-based grid access is not consistently established. Demir et al. [51] proposed an AHP–GIS method for large-scale PV farm site selection in İzmir, Türkiye; however, outputs remain suitability-focused without PV production atlases and grid-development scenarios. Aliabadi et al. [52] integrated technical, economic, environmental, and social analysis for solar energy potential in Qazvin, Iran, using GIS–PVSOL and reporting economic parameters; nevertheless, missing/unclear reporting of lifetime and WACC in the extracted economic summary limits reproducibility. Shi et al. [53] proposed a GIS and AHP–TOPSIS strategy for PV plant siting on gangue hills, strengthening applicability to constrained landforms; however, PV production atlases and grid scenarios are not central to the contribution. Khazael et al. [54] enhanced PV suitability mapping in the Middle East using an optimized deep-learning framework, strengthening predictive screening; yet, feasibility still requires explicit PV yield modelling, grid pathway scenarios, and environmental constraints. Bertsiou et al. [55] developed a GIS–MCDM model for optimal siting of wind and solar parks on Karpathos Island, Greece, strengthening multi-technology planning; however, PV production atlas and grid-access scenarios remain limited. Dinçer et al. [56] enhanced the objectivity of AHP for more reliable solar farm site selection, strengthening weighting robustness; still, the approach remains primarily suitability-based without explicit PV production atlas modelling and scenario grid planning.

A key result of the review is that economic assessment is scarce: among the 46 reviewed studies, only eight explicitly report LCOE-type economics, Imam et al. [13] in Saudi Arabia, Wang et al. [16] in China, Hamad et al. [17] in Afghanistan, Elkadeem et al. [21] in Saudi Arabia, Saraswat et al. [26] in India, Santana-Sarmiento and Velázquez-Medina [27] in Spain, Boube et al. [36] in Niger, and Aliabadi et al. [50] in Iran. Importantly, even within this subset, the transparency of LCOE drivers is uneven: degradation and/or lifetime are frequently not reported, financing assumptions (WACC/discount rate) are not consistently stated, and OPEX definitions vary (percentage of CAPEX vs. $/kW-year), which limits reproducibility and cross-study comparability. Moreover, systematic sensitivity analysis is rarely embedded, although LCOE is highly parameter-dependent (e.g., CAPEX, OPEX, discount rate/WACC, lifetime, degradation rate, and energy yield assumptions); without sensitivity testing, cross-site and cross-study comparisons can be misleading and less decision-relevant.

1.2. Algeria context

Against this methodological background, Algeria represents a

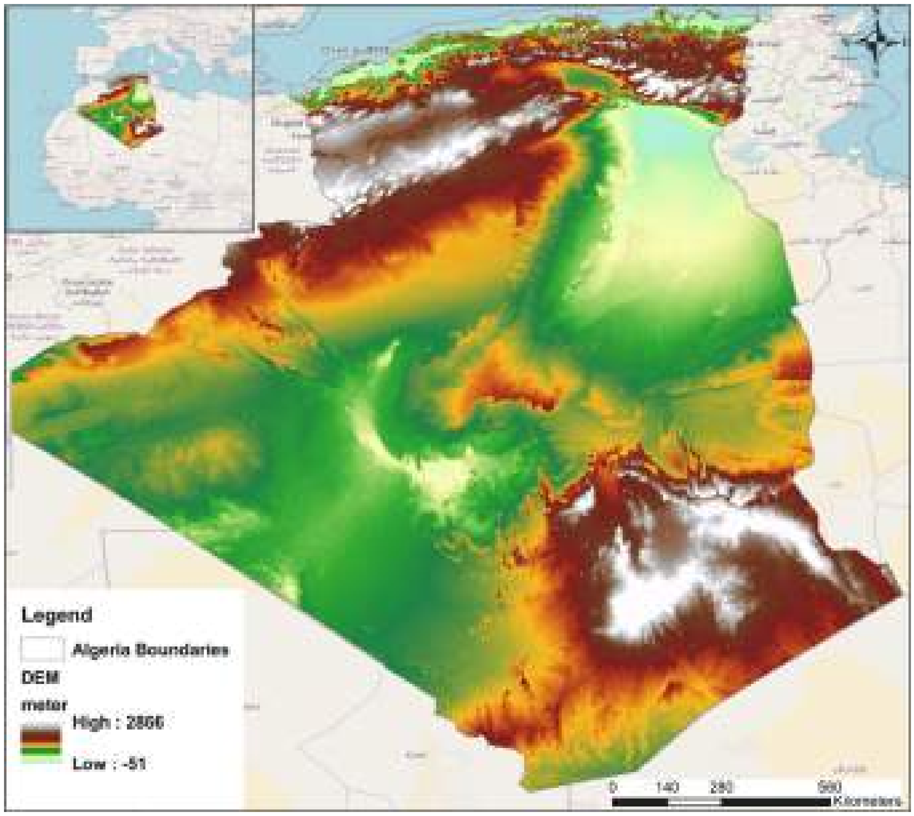

Fig. 1. Location of the study area and geographical context of Algeria.

particularly policy-relevant case because its highest solar resources are concentrated in the Saharan south, whereas population, demand, and grid density are largely located in the northern coastal provinces. Global resource assessments place the Algerian Sahara among the highest global GHI/DNI regimes, indicating substantial technical potential [57]. This resource–load geography creates a persistent north–south mismatch between resource-rich southern basins and northern demand centers.

Policy targets signal intent to mobilize this endowment. Current plans envisage rapid renewable build-out on the order of ~15 GW by 2035, with solar expected to supply a significant share [58]. On the transmission side, SONELGAZ/GRTE has initiated a ~700 km, 400 kV interconnection to link southern systems (PIAT) to the national grid, representing an explicit step toward south-to-north transfer [59]. In parallel, a 2024 MoU with ENI (with Sonatrach and Sonelgaz) is examining the feasibility of a submarine interconnector to Italy, indicating interest in cross-Mediterranean exchange [60]. Prior surveys also identify Algeria as a leading solar resource within the Mediterranean basin, supported by extensive sunshine duration and favorable climatology [14]. The National Renewable Energy Development Program (2011) sets multi-technology ambitions and allocates sizable capacity to PV, while recent statistics report a steadily rising installed base and an expanding pipeline [61].

1.3. Research gap and contributions

Despite Algeria's exceptional solar resources and active policy signals, existing PV siting studies still exhibit limitations that reduce decision usefulness for investment-grade planning. First, several workflows rely on incomplete criteria stacks that omit performance-relevant drivers (e.g., Linke turbidity, sunshine duration/cloudiness, surface albedo, and explicit orientation/tilt representation). Second, the literature largely prioritizes utility-scale siting, with comparatively limited attention to low-/distributed PV opportunities and distribution-level ("low-grid") hosting constraints. Third, PV production mapping is often restricted to a single configuration (horizontal or tilted), and a reproducible national PV production/yield atlas is generally lacking. Fourth, techno-economic and environmental screening is not consistently integrated in a spatially explicit manner that (i) incorporates connection/access cost adders, (ii) applies auditable exclusion masks relevant to Saharan operability (e.g., dunes and moving sands), and (iii) evaluates robustness through sensitivity analysis of key LCOE drivers (e.g., discount rate/WACC, CAPEX, OPEX, lifetime, degradation, and yield). These gaps are particularly consequential under Algeria's north–south resource–load mismatch, where feasible grid-access pathways and environmental operability constraints become first-order determinants of deliverability.

Beyond prior Algerian and MENA GIS-MCDA PV siting studies, which often remain suitability-oriented, the proposed GIS-FAHP-LCOE framework offers an end-to-end, decision-oriented workflow. It combines: (i) high-resolution suitability screening with PV-relevant criteria and auditable exclusion masks, including Saharan operability constraints; (ii) a reproducible PV production atlas for horizontal and optimally tilted configurations; (iii) scenario-based grid-access corridors aligned with Algeria's north–south resource-load mismatch; and (iv) spatial feasibility indicators that integrate discounted LCOE, CO_2/environmental screening, and robustness checks through sensitivity analysis.

To address these gaps, this study proposes a revised, nation-scale PV site-selection framework for Algeria with the following contributions:

1. **High-resolution suitability mapping:** A harmonized 100 m × 100 m GIS database capturing key siting and performance drivers (solar resource and atmospheric conditions, terrain, land use/land cover, protected areas, accessibility, and transmission/distribution grid constraints), combined with expert-elicited FAHP weights and fully documented exclusion/buffer rules.

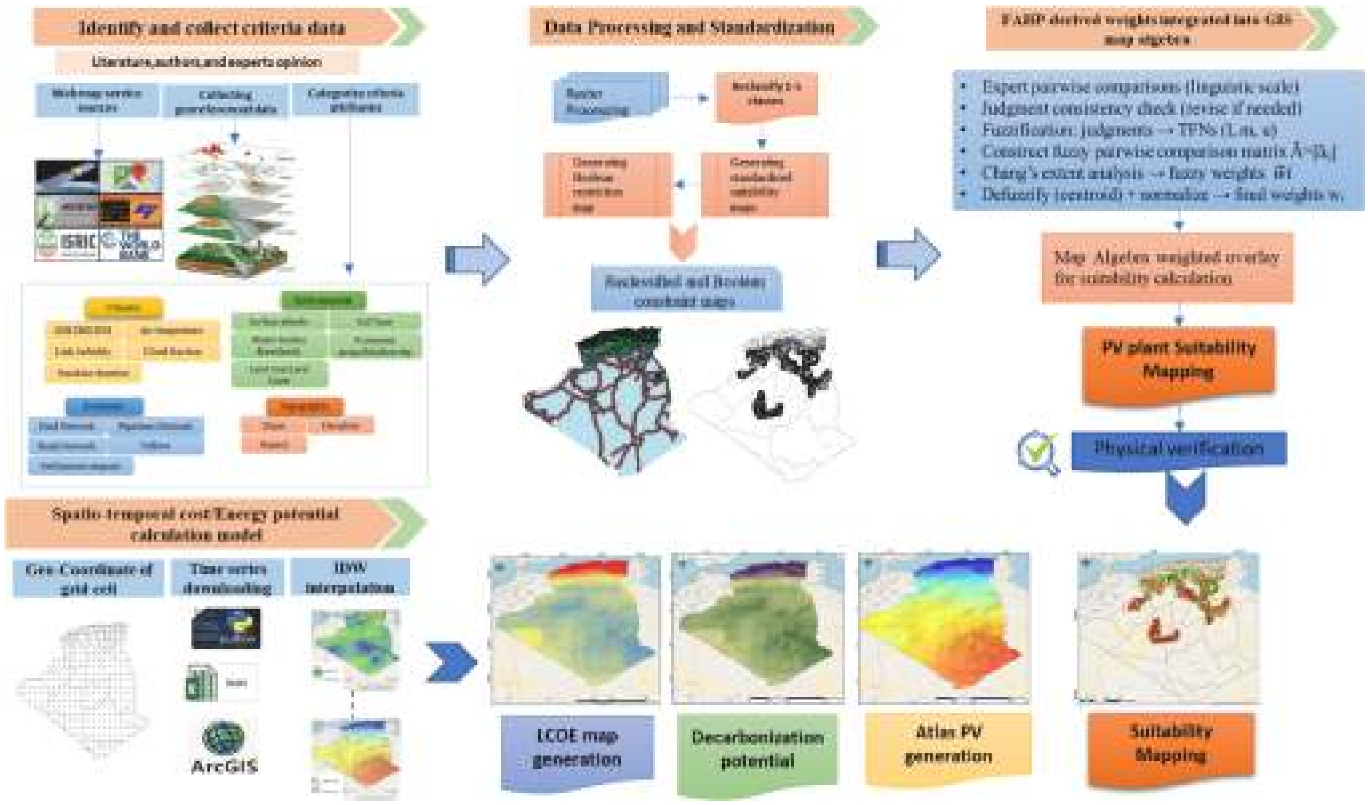

Fig. 2. Workflow of the proposed multi-criteria framework for photovoltaic siting, energy potential, and economic analysis.

2. **Multi-scale deployment scenarios:** Parallel suitability mapping for utility-scale and distributed/low-scale PV, complemented by an infrastructure-independent (“offline”) scenario in which proximity-to-grid/roads/settlements constraints are removed to reveal intrinsically favorable but currently remote clusters.
3. **PV production atlas:** Spatially explicit annual alternating-current (AC) yield maps for horizontal and optimally tilted configurations, based on plane-of-array irradiance.
4. **Transmission expansion assessment:** A grid-scenario analysis evaluating conceptual north–south interconnection pathways and alternative routing toward major load nodes, quantifying how enhanced transmission access can unlock high-quality southern PV resources under realistic land and environmental constraints.
5. **Techno-economic and environmental metrics:** Site-specific discounted LCOE for horizontal and tilted PV including connection/access cost adders, complemented by sensitivity tests across key economic and performance drivers, and a screening-level CO_2 mitigation estimate under a fossil (gas) displacement baseline.

The remainder of the paper is organized as follows. Section 2 describes the study area, datasets, and the adopted methodology, including the GIS–MCDA workflow, exclusion masks, FAHP weighting, and scenario design. Section 3 presents the results, including suitability mapping, the PV production atlas, grid-corridor scenarios, and techno-economic and environmental indicators. Section 4 discusses and validates the findings through comparison with operational and planned photovoltaic power plants and robustness checks. Finally, Section 5 concludes the paper and highlights key implications for large-scale photovoltaic planning and future research directions.

2. Materials and methods

2.1. Study area: Algeria

Algeria is the largest country in Africa (Fig. 1), covering about 2.38 million km^2, with roughly 80% of its territory lying in the Sahara Desert. This gives the country continental-scale land availability in one of the sunniest belts on Earth. Solar resource maps from the Global Solar Atlas show that Algeria’s long-term average global horizontal irradiation (GHI) ranges roughly from 4.6 to 6.6 kWh/m^2/day between the milder Mediterranean north and the high-insolation Saharan south and up to 3,500 h of sunshine annually. Geographically, Algeria’s Mediterranean coastline faces directly toward Europe, making it a natural candidate for renewable-electricity exports. In 2024, state companies Sonatrach and Sonelgaz signed a memorandum of understanding with ENI to study a subsea power interconnection between Algeria and Italy, an infrastructure concept explicitly framed as supporting future low-carbon power exchanges between North Africa and Europe. On the policy side, Algeria’s National Program for the Development of Renewable Energies targets about 15,000 MW of renewable capacity by 2035, aiming for roughly a 30% renewable share in electricity, with around 13.5 GW of solar PV planned by 2030. Recent government announcements confirm that the first 3.2 GW of utility-scale solar plants are scheduled to enter operation from 2025 as the initial phase of this programme.

2.2. Methodology and criteria selection

The proposed framework combines fuzzy Analytic Hierarchy Process (FAHP) and GIS-based multicriteria decision making (MCDM) to identify and rank suitable locations for PV plants. Within this framework, a GIS–MCDM procedure supported by FAHP is used to delineate optimal sites for solar farm development in Algeria. The selection of criteria is grounded in an extensive review of previous PV siting studies and technical guidelines, complemented by the authors' practical experience and structured consultations with specialists in solar energy, power systems, and environmental planning.

To operationalize the analysis, a wide range of spatial datasets was compiled from open-access repositories, national government agencies, and published studies, and harmonized within a common GIS database. Based on these sources and expert consultation, a final set of relevant factors was retained as decision criteria, representing climatic, environmental, topographic, and techno-economic aspects that influence the feasibility and performance of PV projects in Algeria.

These criteria constitute the hierarchical input to the FAHP procedure, where the experts' crisp pairwise judgments are converted into triangular fuzzy numbers (TFNs) to construct the fuzzy-AHP model. The resulting fuzzy weights are then integrated into the GIS-MCDM workflow. In this step, the Raster Calculator and Fuzzy Membership functions within the ArcGIS Spatial Analyst toolbox are employed to process and standardize the thematic layers of all considered criteria, enabling the generation of the final PV suitability map.

All spatial processing and suitability modelling were implemented in *ArcGIS* using the Spatial Analyst extension. To ensure full reproducibility, a fixed processing environment was enforced for all layers: a common coordinate reference system, a unified raster grid at 100 m cell size, identical spatial extent, and a consistent snap raster. Continuous rasters were resampled using bilinear interpolation, whereas categorical layers were resampled using nearest-neighbour assignment to preserve class integrity. All intermediate and final outputs were stored in a structured geodatabase with consistent naming conventions by criterion and scenario.

The workflow (Fig. 2) is organized into two complementary methodological blocks: (i) GIS–MCDA suitability mapping for PV siting under multiple deployment scenarios, and (ii) a spatio-temporal techno-economic and environmental assessment that produces a PV production atlas, LCOE surfaces, and CO_2-avoidance indicators. The main steps are summarized below.

Block 1. GIS–MCDA suitability mapping (PV siting scenarios)

A1. Criteria definition and data acquisition. The criteria influencing PV siting are identified through a focused review of the PV siting literature, expert consultation, and the authors' operational knowledge. Geospatial layers are collected from reputable open-access platforms and national agencies, then grouped into climatic, environmental, topographic, and techno-economic categories.

A2. Data processing, standardization, and constraint design. All datasets are harmonized to a common projection and spatial resolution. Continuous factors are transformed into standardized suitability layers through reclassification into five ordered classes (from extremely suitable to poorly suitable). For proximity-based variables (e.g., roads, transmission lines, settlements), Euclidean distance raster's are generated. In parallel, Boolean restriction masks and buffer-based exclusion zones are constructed to represent land-use and environmental constraints and to implement the study's alternative development scenarios (including variants with and without the soil-type exclusion for dunes and moving sands).

Each criterion layer was converted into a raster suitability surface on the common 100 m grid. Vector datasets (e.g., roads, transmission lines, settlements, protected areas) were first projected to the common Coordinate Reference System (CRS), then transformed into raster layers either by direct rasterization or via proximity surfaces computed using Euclidean distance. Threshold-based exclusion rules were implemented as Boolean masks using buffer operations followed by raster conversion (0 = excluded, 1 = eligible). Continuous suitability factors were standardized by either (i) Reclassify into ordered suitability classes or (ii) Fuzzy Membership functions when monotonic suitability responses were assumed. Final suitability indices were computed in Raster Calculator using weighted linear combination (map algebra). Scenario-specific outputs were then generated by multiplying the continuous suitability index by the corresponding Boolean exclusion masks on a cell-by-cell basis. This step removed restricted areas and produced the final suitability maps.

A3. Weighting and suitability index generation (FAHP + GIS overlay). Expert judgments are translated into pairwise comparison matrices and encoded as triangular fuzzy numbers. The FAHP procedure is applied to derive normalized criterion weights, and consistency is checked to ensure coherent judgments. Final suitability indices are computed in GIS using weighted linear overlay (map algebra), and then combined with the scenario-specific Boolean masks (cell-by-cell) to remove excluded areas and produce the final PV suitability maps for each deployment scenario. A final physical/visual verification step is performed to confirm plausibility.

Block 2. PV atlas, LCOE, and CO_2 assessment (spatio-temporal performance layer)

A1. Hourly climate/resource time-series extraction

Long-term hourly meteorological and irradiance variables were retrieved from the NASA POWER database over a regular 100 km × 100 km grid covering Algeria. The extracted variables included global horizontal irradiance (GHI), ambient temperature, wind speed, and surface albedo, thereby ensuring spatially consistent climatic forcing while preserving seasonal and diurnal variability relevant to PV performance assessment.

A2. PV production atlas construction.

The extracted hourly time series were used to simulate PV electricity generation for both horizontal and optimally tilted photovoltaic configurations. For the tilted case, plane-of-array irradiance was estimated using the Perez anisotropic sky model, with the optimal fixed tilt assigned at each grid point. PV conversion was simulated using the Sandia Photovoltaic Array Performance Model (SAPM), which accounts for effective irradiance, cell temperature, wind-dependent thermal behavior, and angle-of-incidence effects. A representative crystalline-silicon module from the Sandia database (SunPower_SPR_220_BLK_U_-Module_2008_E_) was adopted as a reference technology to ensure spatial consistency and normalized comparison across the national domain.

Annual AC electricity yield was then expressed per unit land area using a 1 km^2 reference surface and assuming 75% land coverage by PV modules, resulting in annual energy-yield maps in $GWh\cdot km^{-2}\cdot yr^{-1}$. The resulting point-based outputs were interpolated to continuous national surfaces and subsequently intersected with the suitable-land masks derived for the different planning configurations, namely the current on-grid scenario, the proposed North–South interconnection scenario, and the off-grid (infrastructure-independent) scenario.

A3. LCOE formulation and assumptions.

The economic performance of PV deployment was evaluated using the levelized cost of electricity (LCOE), expressed in c€/kWh, as follows:

$$LCOE(\text{c€/kWh}) = \frac{CAPEX + \sum_{t=1}^{N}\frac{OPEX}{(1+r)^t}}{\sum_{t=1}^{N}\frac{E_1(1-\delta)^t}{(1+r)^t}} \quad (1)$$

where CAPEX is the total capital investment cost in (€/) for the first year, OPEX is the annual operation and maintenance cost, N is the project lifetime (years), r is the discount rate (WACC), δ is the annual performance degradation rate, and E_1 is the first-year electricity generation (MWh/yr) computed from the simulated capacity factor:

$$E_1 = P.CF.8760 \quad (2)$$

$$\text{CF} = \frac{\text{actual annual energy output}}{\text{maximum possible output at rated power}} \quad (3)$$

with **P** denoting plant rated capacity (MW) and **CF** the annual capacity factor.

A fixed 80 MW plant size was adopted as a representative utility-scale reference project. This assumption was selected to provide a harmonized project frame for national comparison rather than to

Table 1
Economic and technical assumptions used for LCOE calculation.

Parameter	Symbol	value	Unit
Plant rated capacity	P	80	MW
Project lifetime	N	25	years
Discount rate (WACC)	r	7	%
Annual degradation rate	δ	0.25	$\%.yr^{-1}$
Capital expenditure	CAPEX	900	$EUR.KW^{-1}$
Fixed O&M cost	OPEX	0.17% of CAPEX	%
Annual operating hours	H	8760	$h.yr^{-1}$

represent a single plant design. Because the main economic inputs were specified on a normalized basis (e.g., EUR/kW for CAPEX and a fixed proportion of CAPEX for OPEX), the assumed plant size does not determine the spatial ranking of LCOE values. Instead, the mapped variability is driven mainly by differences in PV productivity across locations.

The reported LCOE therefore represents a screening-level plant-gate generation cost under harmonized assumptions. Spatial variability in LCOE is driven mainly by the first-year energy term derived from the PV simulations. Costs related to grid extension, connection reinforcement, road development, logistics, customs duties, and VAT were not embedded directly in the LCOE equation. Instead, infrastructure effects were represented spatially through the scenario-specific suitability masks. This distinction is important because it means that the LCOE maps should be interpreted as comparable generation-cost surfaces, while scenario-based infrastructure constraints are handled separately through land eligibility.

The reference values adopted for the economic assessment, including plant size, CAPEX, fixed O&M cost (OPEX), lifetime, discount rate (WACC), and degradation rate are summarized in Table 1 [62].

For uncertainty analysis, 10,000 Monte Carlo simulations were performed for each eligible grid cell by propagating uncertainty in CAPEX, OPEX, WACC, degradation rate, and annual yield, from which P05, P50, and P95 LCOE values were extracted.

A4. Avoided CO_2 mitigation indicator

The environmental layer was quantified as an indicative avoided CO_2 emissions potential associated with PV electricity generation replacing fossil-based electricity, expressed on an annual per-unit-area basis. The calculation was based on the simulated annual AC electricity yield as [63]:

$$CO_{2,mitigation} = E_{AC}(Kwh) \times 0.28(kgCO_2/kWh) \tag{4}$$

where E_{AC} is the annual PV AC electricity yield.

This formulation was intended to provide an indicative spatial mitigation metric rather than a full life-cycle carbon assessment. Accordingly, the resulting CO_2 maps represent operational substitution benefits under a fixed emissions-intensity assumption and do not include upstream manufacturing emissions, replacement effects, transmission-related emissions, or temporal variations in the carbon intensity of the displaced grid mix.

2.2.1. Criteria

This subsection provides a detailed description of the criteria used to assess the suitability of potential PV plant locations. The selected layers reflect the key climatic, environmental, topographic, and techno-economic factors that influence solar energy production, installation feasibility, and long-term operational performance (Fig. 3).

2.2.1.1. Climatic criteria. 1. Global Horizontal Solar irradiation GHI

Global solar radiation is one of the most decisive criteria for PV site selection, as higher irradiance directly translates into greater electricity generation potential. Studies generally indicate that annual average values around 4.6–4.9 kWh/m^2/day [64,65], ensure economically viable PV operation. In this work, **GHI** is used because it represents the total solar energy received on a horizontal surface, combining both direct normal irradiance (DNI) and diffuse horizontal irradiance (DHI), making it the most appropriate indicator for large-scale PV assessment.

In this study, solar resource information was obtained from the Global Solar Atlas,[1] provided by the World Bank Group and developed by Solargis under the ESMAP program. The GHI layers are derived from satellite-based irradiance time series (10–30 min intervals) and atmospheric modelling, aggregated into long-term annual and monthly averages, and delivered as gridded data with a nominal spatial resolution of 250 m for latitudes between about 60°N and 55°S.

2. Atmospheric temperature t^o

Ambient temperature[2] directly affects PV module efficiency. As temperature increases, panel performance declines, with typical losses of about 0.4–0.5% per °C above the standard test condition of 25 °C [66].

3. Link turbidity factor (TL)

The Link Turbidity Factor quantifies the attenuation of solar irradiance in a cloud-free atmosphere caused by aerosols and water vapor. It is defined as the number of clean and dry "atmospheres" that would produce the same attenuation as the actual atmosphere under consideration [67]. A higher TL value indicates greater atmospheric turbidity and thus lower solar irradiance reaching the surface [68].

In this study, the TL dataset was obtained from global climatology (e.g., via the SoDa Service[3]), which combine satellite-based aerosol optical depth, precipitable water vapor, and ground-based turbidity measurements to generate gridded TL maps at approximately 1° resolution. The incorporation of TL into the site-selection model allows us to account for regions where dust, pollution or moisture significantly reduce available solar radiation, even in otherwise high-irradiance climates.

4. Annual average cloudy days

The annual number of cloudy days[4] is an important criterion for PV site suitability [69], as it reflects periods with reduced solar radiation and consequently lower PV output. Areas experiencing fewer cloudy days generally ensure more stable and higher energy production. In this study, locations with an average of fewer than 170 cloudy days per year were considered suitable for further analysis.

5. Sunshine duration

Sunshine duration data were obtained from the EUMETSAT CM SAF SARAH[5] sunshine duration (SDU) product via the CM SAF Web User Interface. The SDU climate data record is generated for the Meteosat full-disk domain (covering Europe, Africa and the adjacent Atlantic) and is based on visible-channel observations from the MVIRI and SEVIRI instruments onboard the series of geostationary Meteosat satellites. Sunshine duration is not measured directly; CM SAF first retrieves 30-minute direct normal irradiance (DNI) using the Heliosat method and then applies the World Meteorological Organization (WMO) definition of "bright sunshine" (DNI $\geq$ 120 W m^{-2}) to count sunlit intervals. The resulting daily and monthly sunshine-duration sums are provided on a regular 0.05° × 0.05° latitude/longitude grid, corresponding to a spatial resolution of roughly 5 km.

2.2.1.2. Environmental criteria. 1. Surface albedo

Surface albedo represents the fraction of incoming solar radiation reflected by the Earth's surface. Higher albedo surfaces, such as snow, bright soils, or green vegetation, can enhance PV performance by increasing the amount of reflected light available to the modules [70]. In this study, albedo data were sourced from the CM SAF CLARA-A1 dataset,[6] which provides long-term monthly clear-sky albedo derived

[1] https://globalsolaratlas.info/support/about
[2] https://globalsolaratlas.info/support/about
[3] https://www.soda-pro.com/help/general-knowledge/linke-turbidity-factor
[4] https://www.earthenv.org/cloud
[5] https://wui.cmsaf.eu/safira/action/viewProduktSearch
[6] https://wui.cmsaf.eu/safira/action/viewProduktSearch

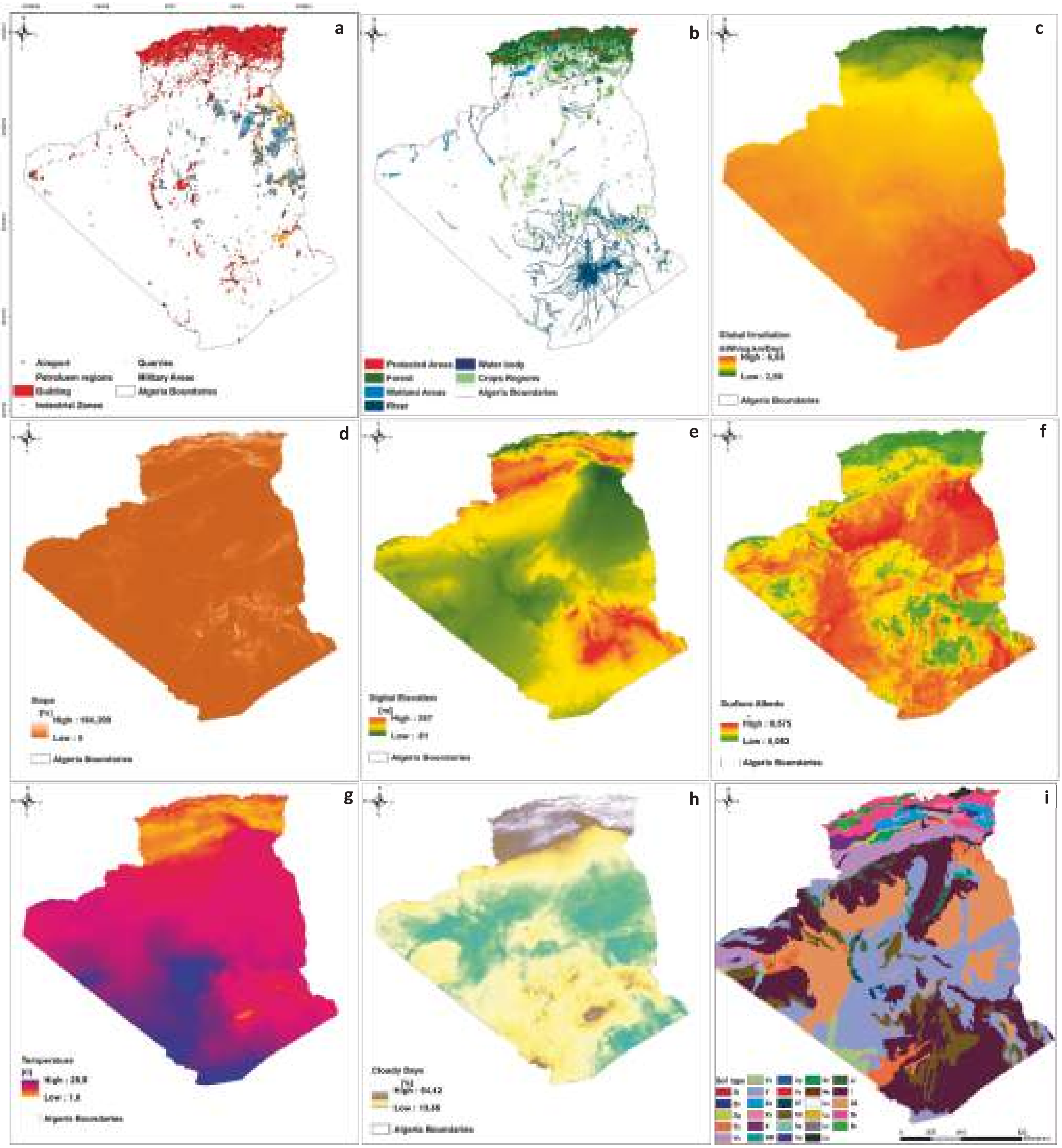

Fig. 3. Input datasets and spatial criteria employed for photovoltaic suitability analysis: (a) anthropogenic/land-use restriction layers; (b) environmental restriction layers; (c) global irradiation; (d) slope; (e) digital elevation; (f) surface albedo; (g) temperature; (h) cloudy days; and (i) soil type. Fig. 3 (continued). Input datasets and spatial criteria used in the photovoltaic suitability analysis: (j) aspect; (k) Linke turbidity; (l) sunshine duration; (m) high-voltage transmission lines; (n) low-voltage distribution lines; (o) major road network; and (p) pipelines.

from AVHRR measurements on NOAA and MetOp satellites. These fields are delivered globally at a 0.25° (~25 km) resolution and represent multi-decadal averages suitable for large-scale PV resource assessment.

2. Soil type

Soil characteristics influence the geotechnical stability, foundation design, and construction feasibility of utility-scale PV plants, especially in regions affected by loose, mobile sands. In this study, soil information was obtained from the Harmonized World Soil Database (HWSD),[7]

[7] https://www.fao.org/soils-portal/data-hub/soil-maps-and-databases/harmonized-world-soil-database-v20/en/

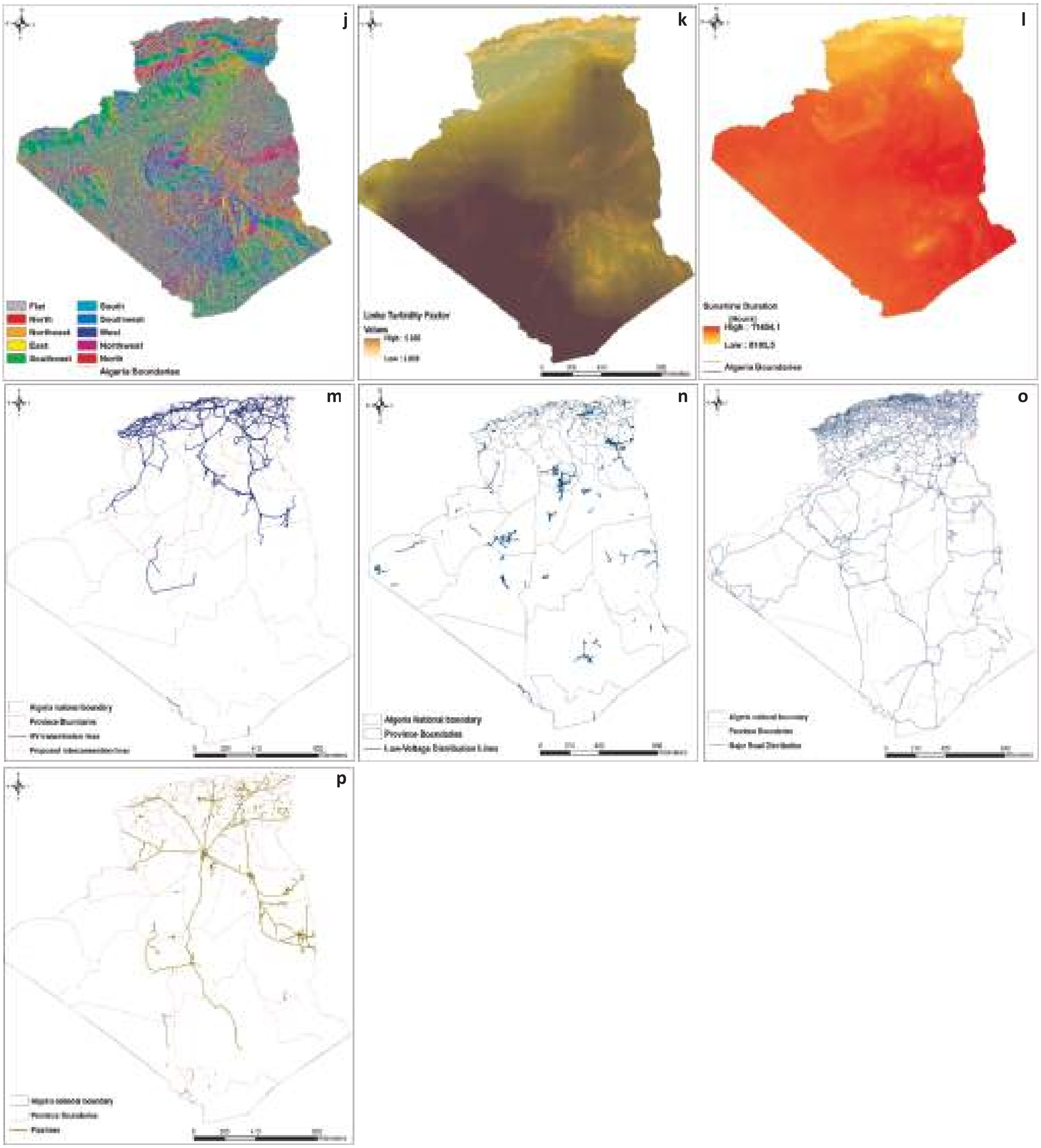

Fig. 3. (*continued*).

which provides a global classification of dominant soil units and associated properties on a regular grid. The resulting soil-type map is used in two ways: (i) as a descriptive environmental layer, and (ii) as a scenario-based constraint. In the latter, areas classified as dunes/moving sand deposits are masked out and treated as unsuitable for PV deployment, yielding an alternative "conservative" suitability map (Index DS, in Fig. 3-k). By performing the GIS–FAHP suitability analysis with and without this soil constraint, the impact of unstable sandy terrains on the spatial distribution of feasible PV sites can be explicitly assessed.

3. Land use /Land cover

Land use and land cover play a critical role in PV siting because solar farms require large, continuous surfaces and can easily conflict with existing land functions. Even where climatic conditions are favorable, unsuitable land use can render a location impractical or undesirable for development [65]. In this study, the LULC criterion is derived from a 10 m high-resolution map generated from the Sentinel-based ESA[8] World Cover product.[9]

Consistent with the majority of PV suitability studies, arid, sparsely vegetated and low-productivity lands are considered the most appropriate for utility-scale installations, while forests, dense vegetation, wetlands, water bodies, urban areas, archaeological sites and military or other restricted zones are treated as exclusion classes. Vegetation is particularly penalized because it reduces the solar energy reaching the modules through shading and also lowers wind speed, which is beneficial for panel cooling. To prevent land degradation and competition with food production, agricultural areas and green lands are not considered for PV deployment. Consequently, wastelands and low-productivity surfaces are prioritized as the preferred LULC types in the suitability analysis [71].

2.2.1.3. Topographical criteria. Topographic conditions modulate the spatial distribution of solar irradiance and strongly affect the constructability and cost of utility-scale PV plants. Variations in elevation, slope and aspect influence the amount of sunlight received at the surface and the need for earthworks, as well as stability, erosion and drainage issues.

1. Elevation

Elevation can influence both PV performance and project costs, as high-altitude sites are often associated with harsher environmental conditions and increased construction and maintenance efforts. In this study, a maximum elevation of 1,500 m is adopted as a practical threshold for site suitability; areas above this limit are excluded from further analysis [30]. The elevation layer was derived from the 30 m Shuttle Radar Topography Mission (SRTM) Digital Elevation Model (DEM) provided by NASA.[10]

2. Slope

3. Slope is a key determinant of both technical feasibility and project costs. Steep terrain increases investment needs for land mobilization and levelling and may aggravate problems related to stability, erosion and drainage. For this reason, flat or gently inclined surfaces are generally preferred for large PV plants. Given the absence of a universally accepted slope threshold in international guidelines and the wide range of limits reported in the literature (typically from 3% up to 30%), this study adopts a 11% slope as a practical restriction.

4. **Aspect** defines how terrain is oriented relative to the sun and thus affects annual solar gains. In Algeria (Northern Hemisphere), south-facing slopes are considered most suitable, followed by south-east and south-west, while east and west have moderate suitability and north-facing slopes are least favorable. The aspect layer derived from the SRTM DEM is reclassified according to this suitability hierarchy for use in the multicriteria evaluation

2.2.1.4. Economic criteria. Techno-economic criteria mainly depend on the location and accessibility of potential PV sites, since these strongly affect construction and grid-connection costs. Proximity to roads lowers the need for new access infrastructure, reduces environmental disturbance, and improves transport and maintenance operations. Distance to the electricity transmission network is also crucial, as remote sites require costly new lines and may suffer higher electrical losses. In addition, the relation to nearby settlements is considered to minimize land-use conflicts while preserving feasible service and connection distances [72,73].

2.2.2. Restrictions used in the study

Restriction criteria define areas where the installation of large-scale PV plants is not allowed and are therefore excluded from the suitability analysis. These zones include locations under legal or environmental protection, land reserved for higher-priority uses, and areas whose physical characteristics prevent infrastructure development. The selection of restrictions was based on a detailed literature review and consultation with domain experts, and was adapted to the specific regulatory and territorial context of the study area.

Table 2 summarizes the restriction variables, their data sources, and the supporting studies that were used as references in this work.

2.3. Multi-criteria decision making with fuzzy AHP

The Analytical Hierarchy Process (AHP) is one of the most widely used MCDM techniques for structuring complex decisions and deriving criteria weights from expert judgement. However, the classical (crisp) AHP assumes that decision makers can express their preferences precisely, which is often unrealistic when dealing with vague or uncertain information. To better capture this imprecision, AHP can be combined with fuzzy set theory [81], giving rise to the Fuzzy AHP (FAHP) approach originally proposed by Van Laarhoven and Pedrycz [82],and later formalized by Chang [83], among others. In FAHP, expert preferences are represented by triangular fuzzy numbers (TFNs) instead of single numerical values, allowing a range of possible importance levels to be modelled for each pairwise comparison.

Linguistic terms such as "equally important", "moderately more important" or "absolutely more important" are associated with *TFNs* (l, m, n) and their reciprocals, ranging from $(1, 1, 1)$ for equal importance up to $(9, 9, 9)$ for absolute dominance, together with the corresponding inverse fuzzy numbers.

Let $\widetilde{A_{ij}} = (l_{ij}, m_{ij}, u_{ij})$ denote the fuzzy judgement expressing the relative importance of criterion *i* with respect to criterion *j*. The FAHP procedure adopted in this study can be summarized in the following steps:

1. Elicitation of pairwise comparisons:

Experts compare each pair of criteria using the predefined linguistic scale. Each verbal judgement is translated into its associated TFN, which provides the lower, most plausible and upper bounds of the relative importance.

2. Construction of the fuzzy comparison matrix:

The TFNs obtained in the previous step populate the fuzzy judgement matrix:

$$\widetilde{A} = \begin{pmatrix} \widetilde{A_{11}} & \cdots & \widetilde{A_{1n}} \\ \vdots & \ddots & \vdots \\ \widetilde{A_{n1}} & \cdots & \widetilde{A_{nn}} \end{pmatrix} \quad (4)$$

where A_{ij} denote the fuzzy judgement expressing the relative importance of criterion *i* with respect to criteria *j*. Each judgement is represented by a triangular fuzzy number.

$\widetilde{A_{ij}} = (l_{ij}, m_{ij}, u_{ij})$

The reciprocal comparison is then given by:

$\widetilde{A_{ij}} = \left(\frac{1}{l_{ij}}, \frac{1}{m_{ij}}, \frac{1}{u_{ij}}\right)$

For multiple experts, the individual fuzzy comparison matrices are combined (here using the geometric mean) to obtain a single collective fuzzy judgement matrix.

Two experts (15–20 years of experience in PV/CSP assessment and planning) provided independent fuzzy pairwise comparison matrices.

[8] https://livingatlas.arcgis.com/landcoverexplorer/#mapCenter=-57.24410%2C-17.91706%2C11.00&mode=step&timeExtent=2017%2C2024&year=2024

[9] https://livingatlas.arcgis.com/landcoverexplorer/#mapCenter=-57.24410%2C 17.91706%2C11.00&mode=step&timeExtent=2017%2C2024&year=2024

[10] https://earthexplorer.usgs.gov/

Table 2
Spatial datasets, resolutions, and restriction thresholds adopted.

Category	Criteria	Data type	Data period	Scale/ resolution	Source	Data accessibility	Threshold /Buffer	References
Environment	Natural Protected Areas, Regional Conservation Areas, Private Conservation AreasPermanent Production Forests.	Vector –polygon shapefile	2023	–	Geofabrik (OSM Algeria extract): https://download.geofabrik.de/africa/algeria.html	Open	≥ 1000 m	[21,31,71,74,75]
	Water bodies	Vector –polygon shapefile	2024	–	Esri Living Atlas (Land Cover Explorer): https://livingatlas.arcgis.com/landcoverexplorer	Open	≥ 1000 m	[21,31,71,74–76]
	Wetlands	Vector –polygon shapefile	2024	–	Esri Living Atlas (Land Cover Explorer): https://livingatlas.arcgis.com/landcoverexplorer	Open	≥ 1000 m	[21,31,74,79,80]
	Soil Type	Raster	1995–2019	1 × 1 km	FAO soils portal (HWSD v2.0): https://www.fao.org/soils-portal/data-hub/soil-maps-and-databases/harmonized-world-soil-database-v20/en/	Open	Dunes and moving sand excluded	Expert
	Petroleum regions	Vector – point shapefile	2024	–	OpenStreetMap (OSM) https://www.openstreetmap.org/	Open	≥ 1500 m	Expert
	Military areas	Vector – point shapefile	2024	–		Open	≥ 1500 m	Expert
	Quarries	Vector –polygon shapefile	2024	–		Open	≥ 2000 m	Expert
	Airports	Vector – point shapefile	2024	–		Open	≥ 1500 m	
Climatic	Global Horizontal Solar irradiation	Raster	1994–2018	250 × 250 m	Global Solar Atlas https://globalsolaratlas.info/map	Open	≥ 1300 Kwh/m^2	[21,67,77–80]
	Temperature	Raster	1994–2018	250 × 250 m		Open	≤ $28C^0$	[31,76]
	Annual average cloudy days	Raster	2000–2014	1 × 1 km	EarthEnv, Global 1-km Cloud Cover climatology https://www.earthenv.org/cloud	Open	≤ 170 days	[76]
	Sunshine duration	Raster	1983–2025	5 × 5 km	EUMETSAT CM SAF, SARAH-3 https://wui.cmsaf.eu/safira/action/viewProduktSearch	Open	–	Expert
	Surface albedo	Raster	1983–2025	5 × 5 km	EUMETSAT CM SAF, CLARA-A3 https://wui.cmsaf.eu/safira/action/viewProduktSearch	Open	–	Expert
Topographical	Elevation	Raster	2000	30 × 30 m	USGS EarthExplorer https://earthexplorer.usgs.gov/	Open	≤1.5 km	[25,28,37,76]
	Slope	Raster	2000	30 × 30 m		Open	≤ 11%	[21,28,37,76]
	Aspect	Raster	2000	30 × 30 m		Open	–	[21,31,69,80]
Economic	Power transmission lines	Vector –lines shapefile	–	–	Official government data (Algeria transmission network / Sonelgaz)	Restricted	Exclusion buffer of 100 m from both sides; sites > 50 km from line are excluded.	[21,31,71,75]
	Major Road	Vector –lines shapefile	–	–	OpenStreetMap (OSM) https://www.openstreetmap.org/	Open	Exclusion buffer of 500 m from both sides; sites > 50 km from line are excluded.	[21,28,37,80]
	Distance to settlement areas(m)	Raster	2024	30 × 30 m	Esri Living Atlas (Land Cover Explorer / settlement layer, 2024) https://livingatlas.arcgis.com/landcoverexplorer/	Open	Exclusion buffer of 1 km from both sides; sites > 50 km from line are excluded.	[21,31,69,71,76]

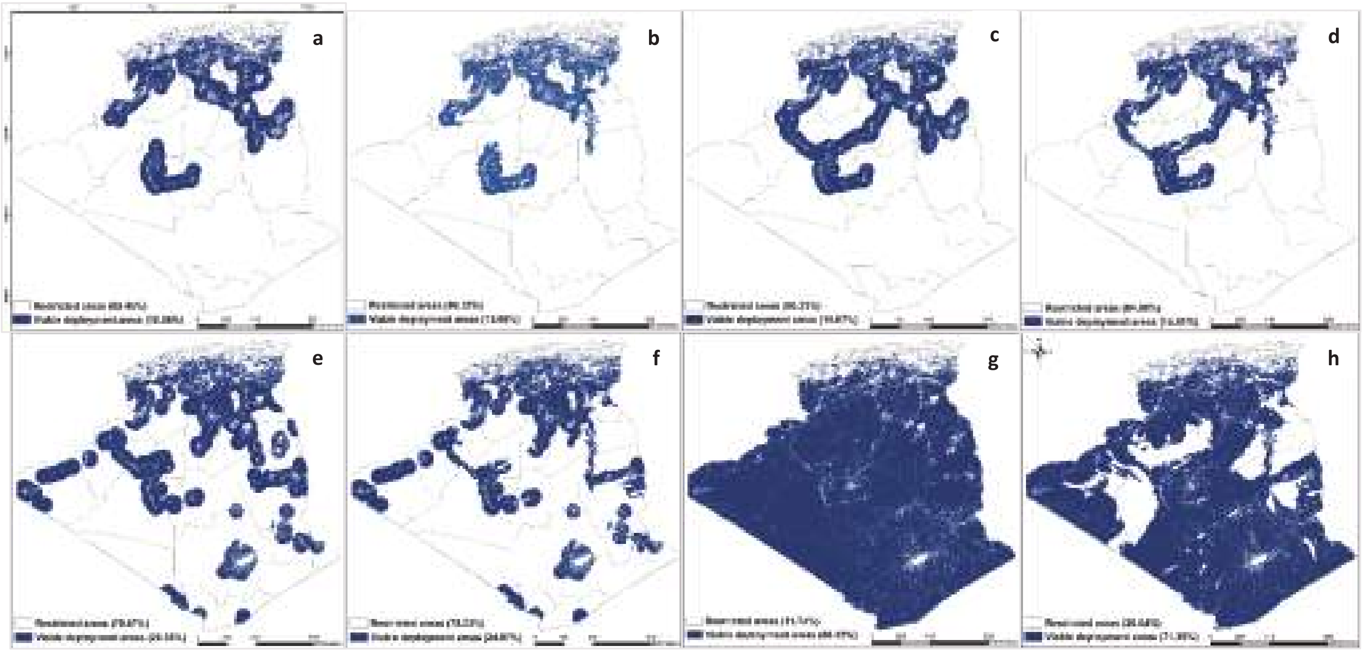

Fig. 4. Spatial distribution of restricted and viable deployment areas under different constraint scenarios, shown with and without soil-type exclusion: (a and b) high-voltage grid-connected scenario, (c and) proposed interconnection-grid scenario, (e and f) low-suitability PV plant scenario, and (g and h) unconstrained national suitability scenario.

The collective fuzzy judgement matrix was obtained using geometric mean aggregation (AIJ) applied component-wise to the triangular fuzzy numbers (l,m,u), which preserves reciprocity in group AHP/FAHP.

3. Derivation of fuzzy criterion weights.

Following the fuzzy geometric mean method, the synthetic importance of each criterion iii is computed as:

$\widetilde{r_i} = \left(\prod_{j=1}^{n}\widetilde{A_{ij}}\right)^{\frac{1}{n}}, i = 1, \cdots, n$ (5)

and normalized with respect to the sum of all of $\widetilde{r_i}$:

$\widetilde{w_i} = \widetilde{r_i}\otimes(\widetilde{r_1}\oplus\widetilde{r_2}\oplus\cdots\oplus\widetilde{r_n})^{-1} = (l_{wi}, m_{wi}, u_{wi})$(6)where $\otimes$ and $\oplus$ denote fuzzy multiplication and addition,respectively. This yields a TFN weight for each criterion.

4. Defuzzification and normalization.

To obtain crisp weights suitable for subsequent GIS operations, each fuzzy weight is defuzzied by taking the mean of its three parameters:

$M_i = \frac{l_{wi}+m_{wi}+u_{wi}}{3}$(7)

The final normalized weight of criteria i then given by:

$N_i = \frac{M_i}{\sum_{k=1}^{n} M_k}$, ensuring that $\sum_i N_i = 1$

5. Consistency assessment.

To verify the reliability of the expert judgements, a consistency analysis analogous to that used in classical AHP is carried out. The crisp approximation of the judgement matrix is used to estimate the maximum eigenvalue λ_{max} and the associated Consistency Index (CI):

$CI = \frac{\lambda_{max}-N}{N-1}$(8)

The Consistency Ratio (CR) is obtained as

$CR = \frac{CI}{RI}$(9)where RI is the average random index for a matrix of size n. A value of $CR < 0.10$ is generally regarded as indicating an acceptable level of consistency; otherwise, the pairwise comparisons should be revisited with the experts.

3. Results and interpretation

3.1. Areas with restricted access

The exclusion masks for the different scenarios are presented in Fig. 4. Depending on the combination of constraints applied, between 17.9 % and 87.6 % of Algeria is excluded from potential development, highlighting the strong influence of environmental and techno-economic limits on PV deployable land.

Under the existing high-voltage grid corridor, constraints are the most severe. Without the soil mask, about 84.8% of the territory is restricted and only 15.2% remains viable. When the dune/moving-sand exclusion is added, the restricted share rises to 87.6% and the viable area falls to 12.4%.In the proposed grid-extension scenario, the restricted area decreases to 78.8 % (viable 21.2 %) and to 82.8 % (viable 17.2 %) when soil instability is also considered, showing that targeted grid expansion significantly enlarges the technically accessible resource.

The large off-grid PV scenario is the most permissive: only 17.9 % of the country is excluded without soil constraints (viable 82.1 %), while the soil mask increases restrictions to 32.9 % (viable 67.1 %). For small-scale PV plants, which must remain near infrastructure and settlements, the restricted share reaches 72.9 % (viable 27.1 %) and 76.8 % (viable 23.2 %) without and with the soil mask, respectively. Overall, grid-related constraints dominate the loss of area, while the dune/moving-sand exclusion further trims the potential, especially in desert regions where solar resource is highest.

3.2. PV suitability surfaces and spatial patterns

The FAHP–GIS framework produced national-scale PV suitability maps that integrate more than sixteen climatic, environmental, topographic and techno-economic criteria. For each experiment, the composite suitability index was reclassified into five categories (extremely, highly, moderately, low and poorly suitable), which facilitates comparison between scenarios and with previous GIS–MCDM studies.

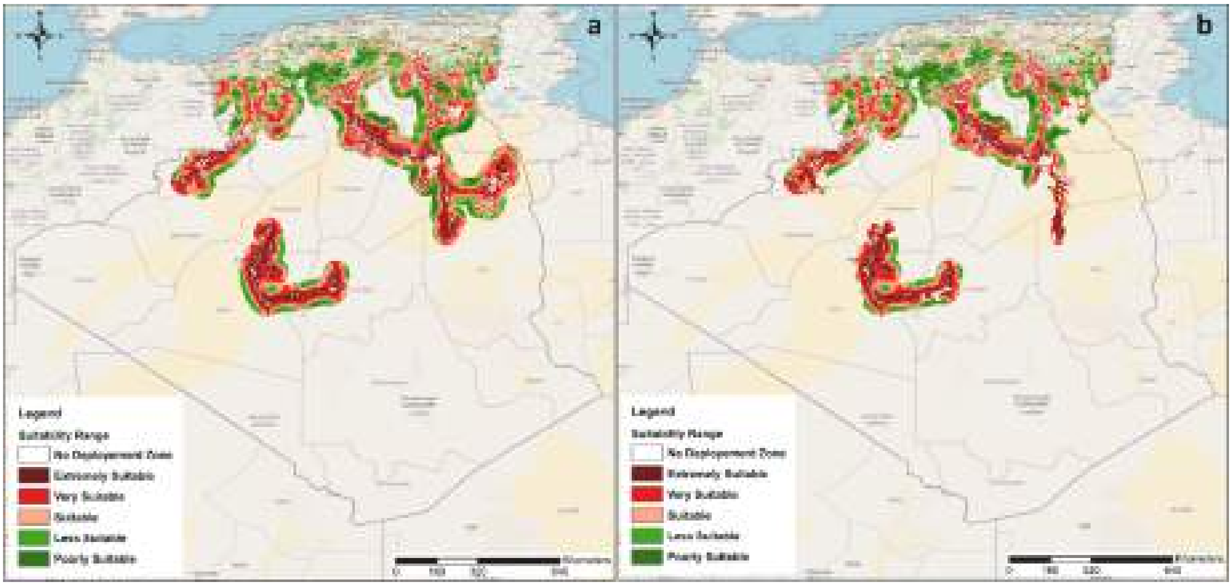

Fig. 5. PV suitability maps for the utility-scale on-grid PV deployment scenario in Algeria: (a) baseline on-grid suitability map; (b) on-grid suitability map with soil-type mask exclusion (dunes and moving sands).

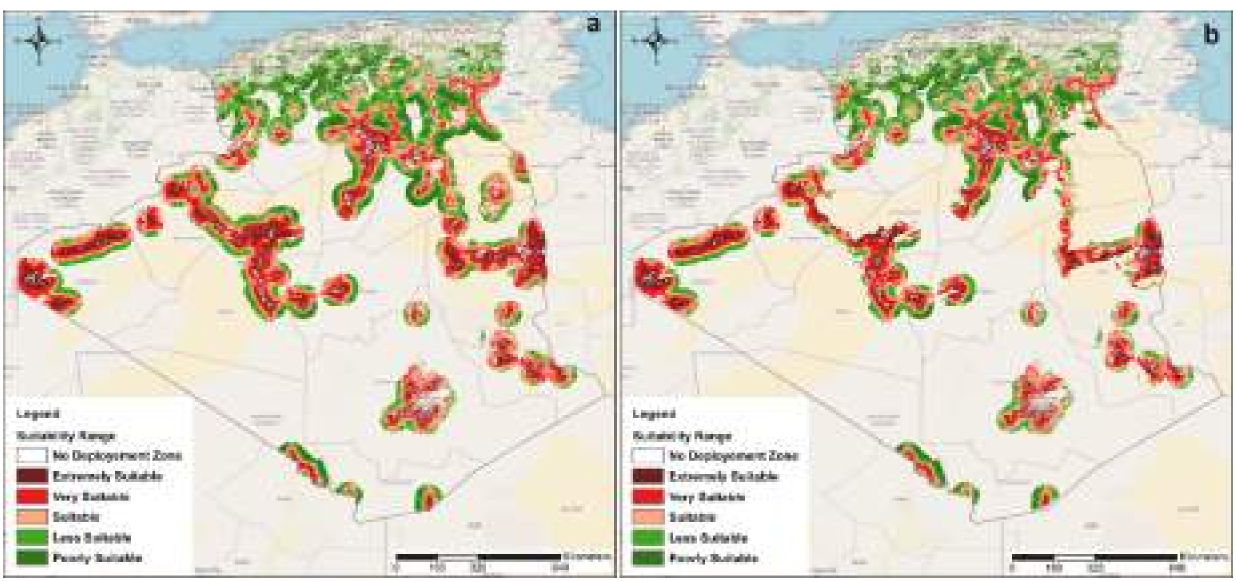

Fig. 6. PV suitability maps for the small-scale on-grid PV deployment scenario in Algeria: (a) baseline on-grid suitability map; (b) on-grid suitability map with soil-type mask exclusion (dunes and moving sands).

3.2.1. Grid-connected suitability under the current network (utility-scale and low-scale)

To facilitate direct visual comparison, the baseline and soil-constrained suitability maps are presented as paired subfigures for each deployment scale. Under the utility-scale, current high-voltage (HV) grid configuration, the suitability surface reflects a dual constraint: strong biophysical potential is necessary, but it becomes actionable only where connection to the existing transmission backbone remains technically realistic. As shown in Fig. 5(a and b), the highest suitability classes (ES–VS) are most pronounced in Saharan high-resource clusters, where solar conditions are inherently favorable, yet their spatial continuity is interrupted and channelized by the limited footprint of the present HV network. In contrast, the northern belt is dominated by lower suitability classes (often LS–PS), with only localized higher-suitability pockets, reflecting the cumulative effect of land-use restrictions, denser environmental constraints, and less advantageous PV performance conditions relative to the Sahara. This pattern indicates that, under the current utility-scale grid-connected configuration, the key limitation is not land availability alone, but rather the availability of grid-accessible high-quality land suitable for bankable large-scale deployment.

The low-scale (distribution-/local grid-connected) scenario exhibits a different spatial logic and a more dispersed suitability structure Fig. 6 (a and b). Here, proximity to settlements and lower-capacity infrastructure becomes more influential, shifting suitability toward demand-proximate corridors and producing many smaller, spatially distributed hotspots rather than a few large contiguous hubs. This dispersion is not a weakness; it highlights a complementary role for low-scale PV in Algeria: it can support incremental electrification needs, including remote communities and agricultural activity (e.g., pumping, cold storage, and local processing), where modular deployment reduces reliance on long-distance transmission reinforcement. In other words,

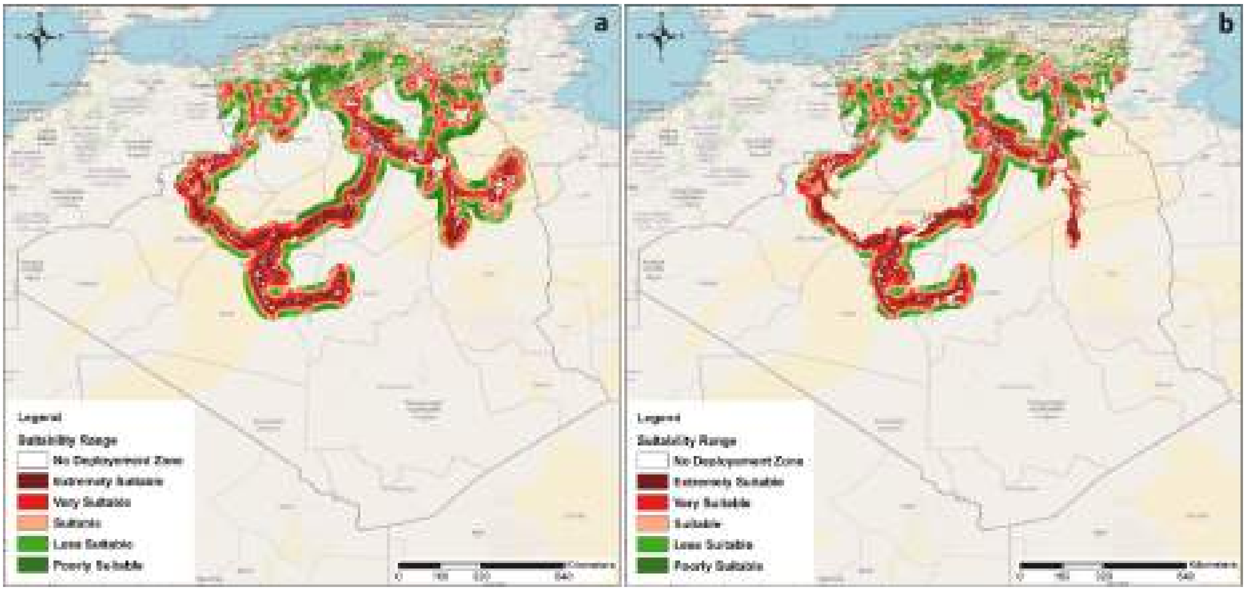

Fig. 7. PV suitability maps for the utility-scale North–South interconnection scenario in Algeria: (a) baseline suitability map; (b) suitability map with soil-type constraint.

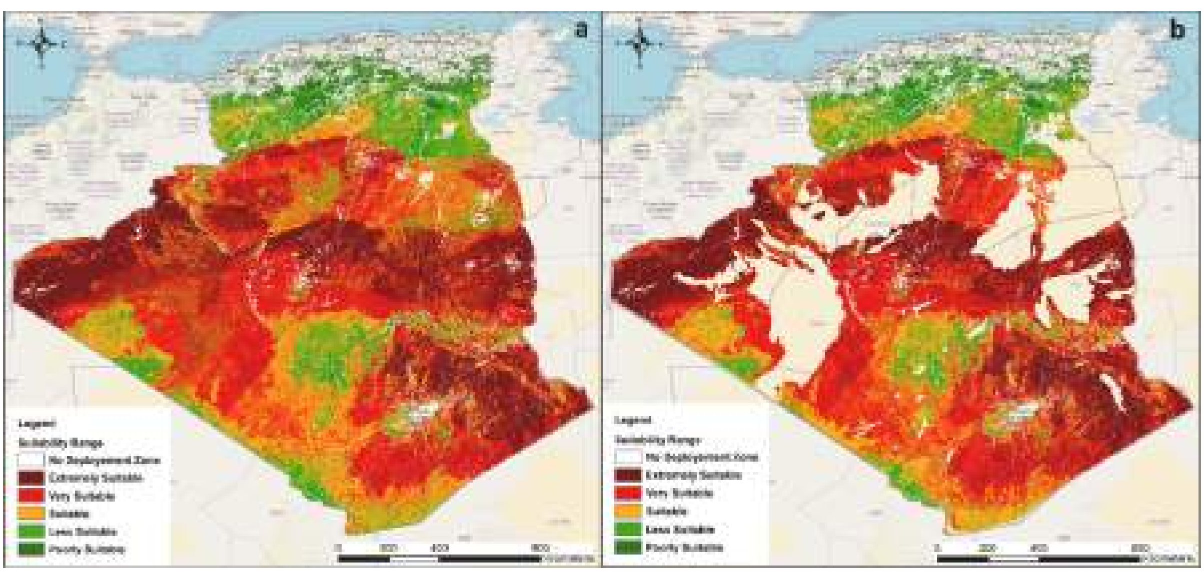

Fig. 8. PV suitability maps for the utility-scale off-grid PV scenario in Algeria: (a) baseline infrastructure-independent suitability map; (b) infrastructure-independent suitability map with soil-type constraint.

while utility-scale siting is constrained by transmission reach, low-scale PV can track access and demand geography, offering a practical pathway for decentralized clean-energy uptake alongside bulk generation projects.

Finally, across both grid-connected cases, the soil-type exclusion (dunes and moving sands) produces a clear and systematic reduction of ES–VS land (Fig. 5(a) with Fig. 5(b) and Fig. 6(a) with Fig. 6(b)), especially within dune-dominated Saharan sectors. This confirms that geomorphological stability is not a secondary detail in arid-region PV planning: excluding unstable sandy terrains can materially reshape where “high suitability” remains technically credible, strengthening the investment relevance of the resulting suitability products compared with assessments that implicitly assume uniform desert stability.

3.2.2. Utility-scale suitability under the proposed North–South grid-connection scenario

The proposed North–South grid-extension scenario is motivated by Algeria’s structural spatial mismatch: electricity demand is concentrated in the northern coastal and highland belt, whereas the highest PV production potential is located in the Saharan south. Under the current HV network, this mismatch translates into a practical bottleneck large parts of the best-performing southern resource clusters remain weakly connectable or economically disadvantaged due to transmission distance.

The resulting suitability maps (Fig. 7a and b) show that extending the grid southward relaxes this constraint and enables a clearer emergence of continuous ES–VS corridors deeper into the Sahara. Importantly, the improvement is not only in the quantity of connectable land, but in the quality of accessible land: the proposed corridors increase the share of high-resource sites that become realistically integrable, shifting

Table 3
Sensitivity analysis of photovoltaic suitability classes under different weighting schemes.

Scenario	Weighting scheme	Soil exclusion (dunes & moving sand)	ES-(Areas km^2 & %)	VS –(Areas km^2 & %)	S –(Areas km^2 & %)	LS –(Areas km^2 & %)	PS –(Areas km^2 & %)
Utility-scale PV—Existing grid	Expert FAHP	No	40,75810.96 %	88,26823.17 %	115,45630.31 %	96,39725.31 %	38,94110.22 %
		Yes	33,87910.75 %	69,92022.2 %	93,42429,66 %	83,58326.54 %	34,11110.83 %
	Equal Weight	No	91,342.23.99 %	123,O78 32.32 %	99,40126,1%	48,10112,63%	18,797 4,93 %
		Yes	81,39325.85	106,15633.71	81,07425.75	34,71611.02	11,4943.65
	Literature Weight	No	50 62913.286	97 57925.606	112 15329.430	81 20421.309	39 51710.370
		Yes	39 77712.622	78 64524.95	90 92828.85	70 24322.289	5 54011.277
Utility-scale PV—Proposed N–S grid	Expert FAHP	No	53,32211.77	104,09722.98	127,53528.15	117,03925.83	50,99211.25
		Yes	39,*564*.10.797	77,15021.054	101,78327.77	101,04627.57	46,88212.79
	Equal Weight	No	108,17223.88	96,43421.29	126,42627.91	107,90023.82	13,9483.08
		Yes	96,10126.23	82,49422.51	102,56327.99	69,90519.08	15,2604.16
	Literature Weight	No	57 17212.61	109 79624.22	135 99130.00	104 18922.98	46 08810.17
		Yes	46 04312.56	86 83223.68	106 60729.07	86 00223.45	41 13611.22

Note: ES = extremely suitable, VS = very suitable, S = suitable, LS = low suitability, PS = poorly suitable, ND = no-deployment zone.

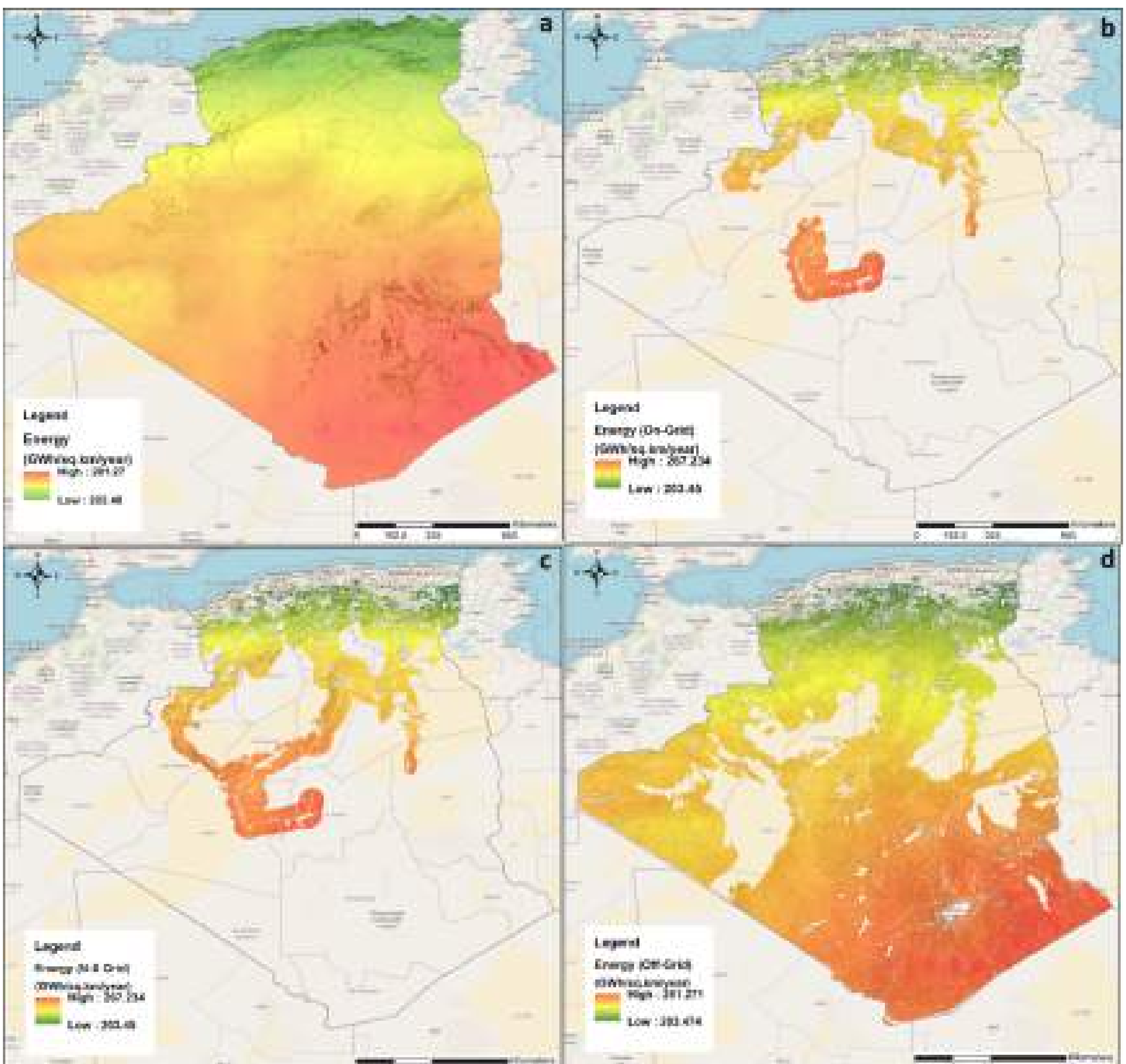

Fig. 9. Annual AC energy-yield maps for horizontal photovoltaic systems in Algeria under different planning configurations: (a) national unconstrained PV atlas; (b) energy-yield distribution under the current on-grid suitability scenario; (c) energy-yield distribution under the proposed North–South grid-connection scenario; and (d) energy-yield distribution under the off-grid (infrastructure-independent) scenario. Units: GWh·km^{-2}·yr^{-1}.

suitability from isolated pockets near existing lines toward strategic corridor-aligned clusters.

The soil-type exclusion remains a critical refinement under this scenario (Fig. 7a vs. Fig. 7b). Removing dunes and moving sands

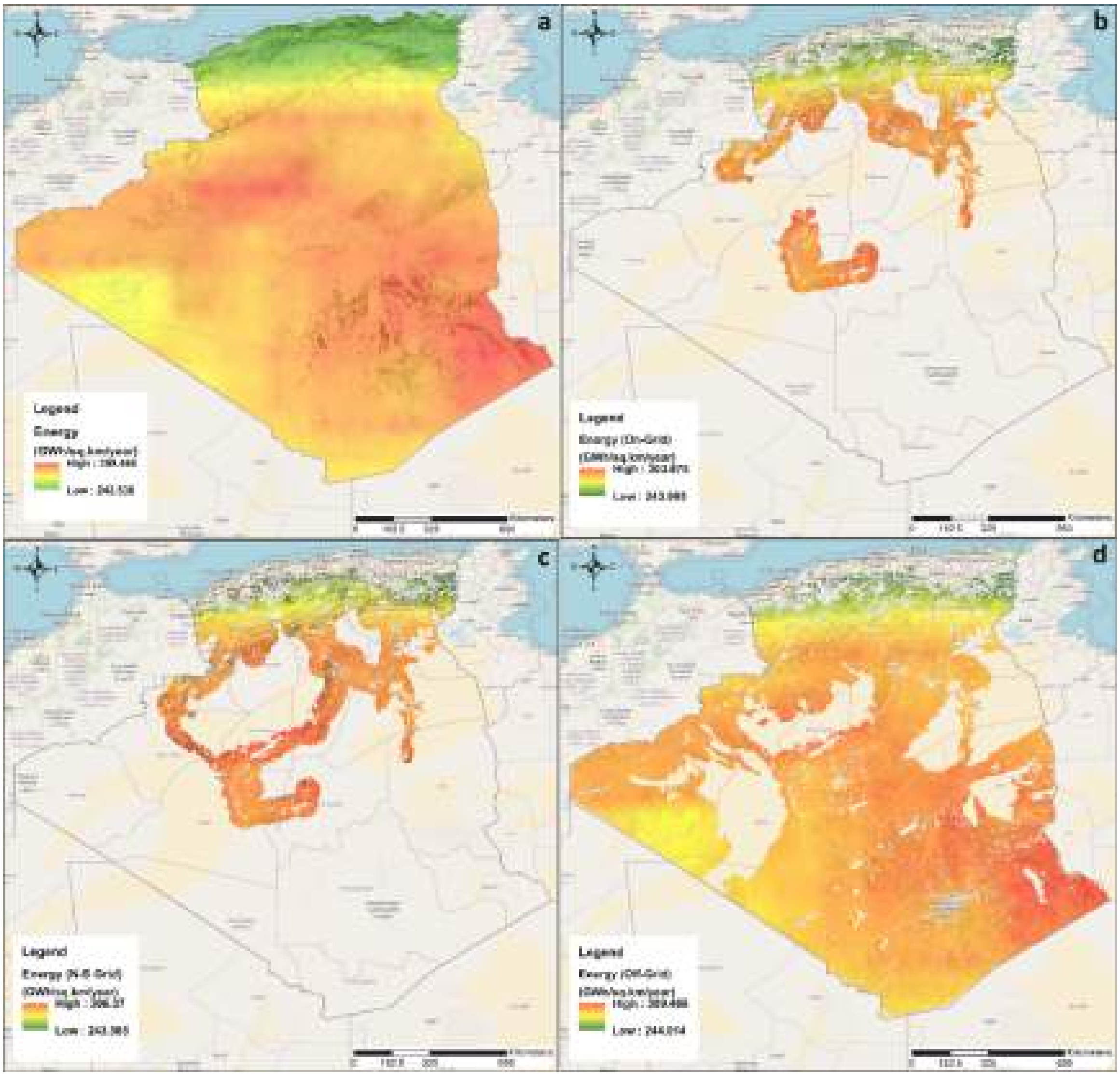

Fig. 10. Annual AC energy-yield maps for horizontal photovoltaic systems in Algeria under different planning configurations: (a) national unconstrained PV atlas; (b) energy-yield distribution under the current on-grid suitability scenario; (c) energy-yield distribution under the proposed North–South grid-connection scenario; and (d) energy-yield distribution under the off-grid (infrastructure-independent) scenario. Units: GWh·km^{-2}·yr^{-1}.

produces a more conservative but more realistic representation of deployable land by filtering out geomorphologically unstable sectors that may appear attractive energetically but carry elevated construction and O&M risks. This is particularly important when planning new corridors, because expansion can otherwise "unlock" areas that are high-yield in theory but problematic in practice. Applying the soil constraint helps steer corridor development toward high-resource and stable land units, improving investment robustness.

Overall, Fig. 7 indicates that the proposed North–South interconnection provides a plausible pathway to reconcile demand geography in the north with production geography in the south while maintaining realistic land and geomorphological constraints. This supports its value as a planning tool for accelerating utility-scale PV deployment, where the objective is to prioritize sites that simultaneously deliver high yields, feasible grid integration, and durable operability.

3.2.3. Offline (infrastructure-independent) suitability and intrinsic biophysical potential

The offline scenario removes distance-to-grid, road-access, and settlement proximity from the suitability computation in order to isolate Algeria's intrinsic biophysical potential for PV deployment. This configuration is intentionally idealized: it answers the question "where would PV be most suitable if infrastructure constraints were not limiting?" The resulting maps (Fig. 8a and b) therefore highlight the dominant role of resource–environment conditions (irradiation regime, atmosphere, terrain, land cover, and protected-area constraints) rather than accessibility.

A clear outcome of Fig. 8(a and b) is that the highest suitability classes expand markedly across the Saharan domain, confirming that large southern areas remain fundamentally attractive for PV on purely biophysical grounds. In contrast, the northern belt becomes comparatively more heterogeneous, reflecting stronger land-use competition, denser environmental exclusions, and less favorable combined conditions than the deep south. In other words, the offline case reveals that the main limitation of many high-quality Saharan clusters is not the resource itself, but the current lack of enabling infrastructure.

Beyond mapping potential, the offline scenario provides an upper-bound benchmark for interpreting grid-constrained results. By comparing offline suitability with the current-grid and proposed grid-extension cases, it becomes possible to distinguish "intrinsically suitable but currently inaccessible" zones from areas that remain limited even without infrastructure constraints. This benchmark role is

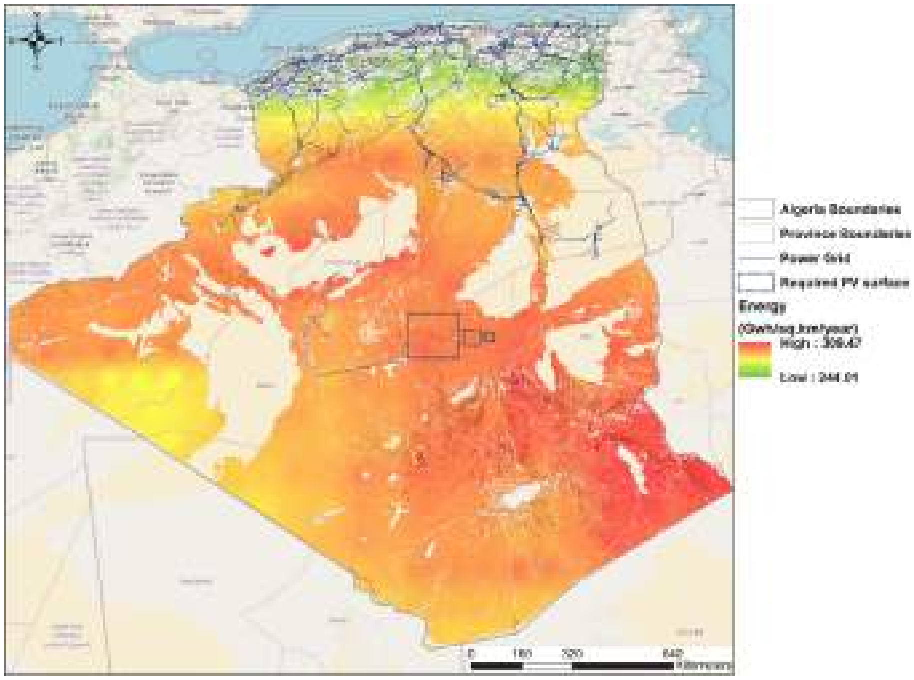

Fig. 11. Large-scale photovoltaic energy potential, required land area for electricity demand supply, and power grid context.

important for planning, because it shows where transmission expansion would yield the largest marginal gains by converting already-high intrinsic potential into bankable, connectable utility-scale opportunities.

The soil-type constraint is particularly informative in the offline setting (Fig. 8a vs. Fig. 8b). Excluding dunes and moving sands reduces suitability in geomorphologically unstable sectors that can otherwise appear attractive due to strong irradiation. This separation between resource-rich land and deployable land prevents systematic over-estimation of PV opportunity in desert environments and reinforces the need to treat geomorphological stability as an explicit siting constraint rather than an implicit assumption.

3.2.4. *Sensitivity of utility-scale suitability areas to weighting assumptions and soil-stability constraints*

Table 3 quantifies how the mapped areas of each suitability class change under (i) the existing high-voltage grid and (ii) the proposed North–South (N–S) grid-extension scenario, while varying both the weighting scheme (expert FAHP, equal weights, literature weights) and the application of the soil-stability exclusion (dunes and moving sands). This sensitivity step is important because it separates effects driven by preference/weight choices from effects driven by an explicit physical constraint (geomorphological instability).

Across both grid contexts, the absolute areas are clearly weight-dependent. Equal weighting systematically produces a much larger "top-end" allocation (ES–VS) than the expert and literature schemes. For the existing-grid case without soil exclusion, ES–VS reaches 214,420 km^2 under equal weights, compared with 129,026 km^2 (expert FAHP) and 148,208 km^2 (literature). This confirms that the quantitative share of "prime" land is not an invariant output of GIS–MCDA; it depends strongly on how trade-offs between criteria are represented, reinforcing the need for transparent justification of weights when suitability results are used for investment screening.

The soil-stability exclusion introduces a second, independent source of variation that consistently reduces deployable area across all weighting schemes and both grid contexts. For example, under expert FAHP, the existing-grid ES-VS area decreases from 129,026 km^2 to 103,799 km^2 after dunes and moving sands are excluded. Under the proposed N-S grid, it decreases from 157,419 km^2 to 116,714 km^2. Similar reductions are observed for the literature-based weights, from 148,208 km^2 to 118,422 km^2 in the existing-grid case and from 166,968 km^2 to 132,875 km^2 in the proposed-grid case. Importantly, the exclusion does not only remove marginal land; it also contracts parts of the highest classes, showing that geomorphological stability can materially reshape where "bankable" PV is expected in desert environments. When comparing the two grid contexts, the proposed N–S corridor shows a robust benefit under the expert and literature weighting schemes, i.e., the classes that most closely reflect informed trade-offs rather than an unweighted average. Without soil exclusion, ES–VS increases by +28,393 km^2 under expert FAHP (129,026 to 157,419 km^2) and by +18,760 km^2 under literature weights (148,208 to 166,968 km^2). With soil exclusion applied, the improvement remains: +12,915 km^2 for expert FAHP (103,799 to 116,714 km^2) and +14,453 km^2 for literature weights (118,422 to 132,875 km^2). These deltas indicate that the proposed corridor does not merely add connectable land; it increases access to higher-quality land even after removing geomorphologically unstable terrain. Under equal weighting, the ES–VS totals do not increase relative to the existing grid, highlighting that this scheme can alter the scenario ranking and redistribute land among classes in a way that is less consistent with infrastructure-planning logic. This reinforces a practical interpretation of Table 3: while all weighting approaches are informative for sensitivity purposes, decision support should rely primarily on expert-structured or literature-grounded weights, and should explicitly report how alternative weighting choices influence the headline areas. Overall, Table 3 supports two main conclusions: (1) suitability-area totals are sensitive to weighting assumptions, so weight transparency is essential; and (2) the strategic advantage of the proposed N–S grid-extension remains evident once expert/literature trade-offs and soil stability are accounted for, strengthening the case for coordinated transmission planning to unlock high-resource Saharan clusters under realistic land constraints.

3.3. *PV Atlas: spatial distribution of solar resource and PV power density*

To complement the suitability assessment, a national-scale PV Atlas was developed to quantify the theoretical and technical electricity-production potential of photovoltaic systems across Algeria under

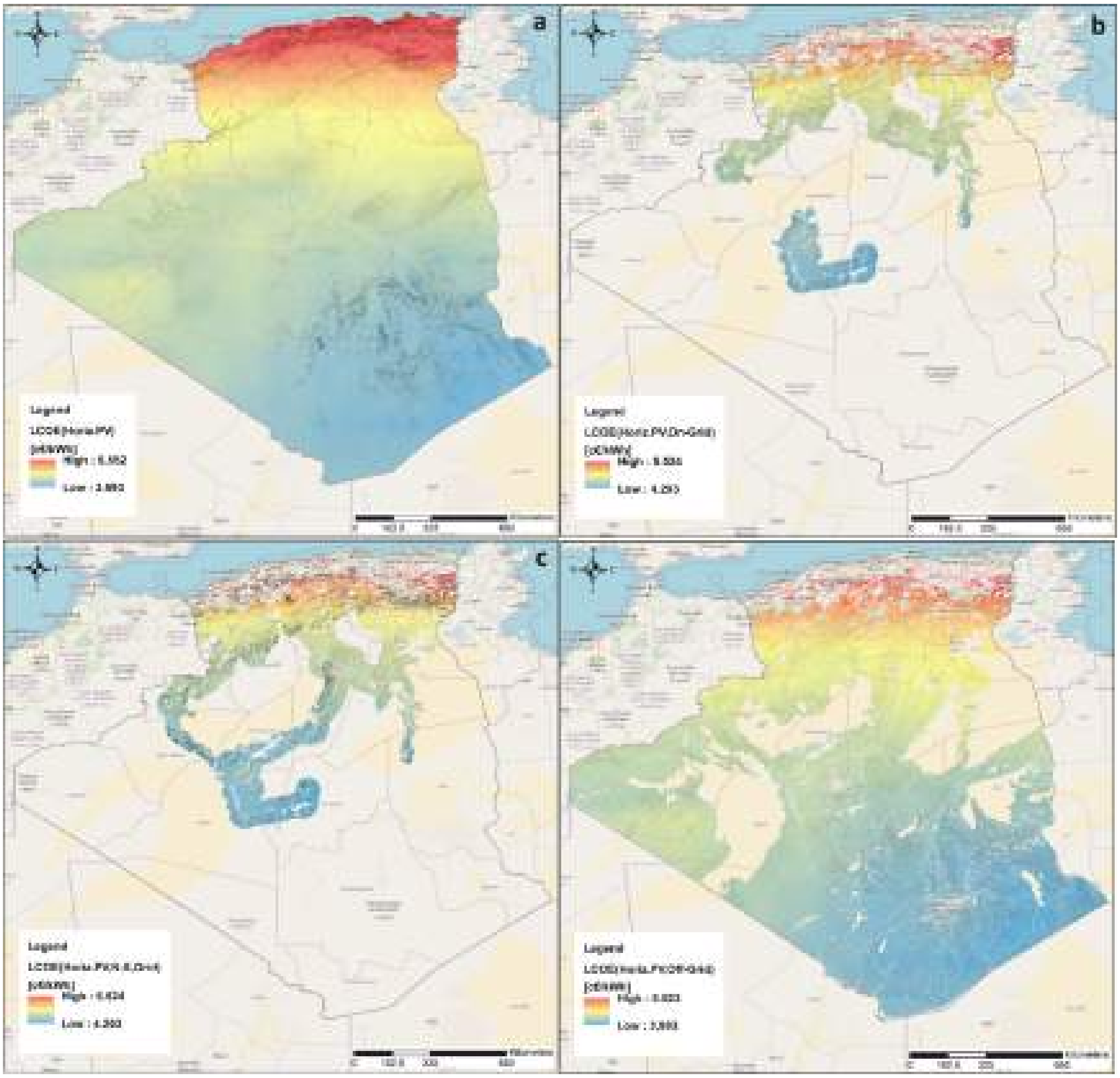

Fig. 12. Spatial distribution of the levelized cost of electricity (LCOE) for utility-scale horizontal photovoltaic systems in Algeria under different planning configurations: (a) national unconstrained LCOE surface; (b) LCOE distribution under the current on-grid scenario; (c) LCOE distribution under the proposed North–South grid-connection scenario; and (d) LCOE distribution under the off-grid (infrastructure-independent) scenario. Units: c€/kWh.

standardized and reproducible assumptions. Hourly meteorological forcing was obtained from the NASA POWER database, including global horizontal irradiance (GHI), air temperature, wind speed, and surface albedo, and sampled over a regular 100 km × 100 km grid covering the national territory. For the tilted configuration, plane-of-array irradiance was derived using the Perez anisotropic sky model [84], with the optimal fixed tilt assigned to each grid point. PV conversion was simulated using the Sandia Photovoltaic Array Performance Model (SAPM) [85], which relates module output to effective irradiance and cell temperature while accounting for major operating effects, including wind-dependent thermal behavior and angle-of-incidence response. A representative crystalline-silicon module from the Sandia database (SunPower_SPR_220_BLK_U_Module_2008_E_) was selected as the reference technology (221.38 W at STC; 1.244 m^2 aperture area) in order to ensure spatial consistency and to report normalized performance rather than plant-specific designs. Annual AC yield was expressed per unit land area using a 1 km^2 reference surface and assuming 75% land coverage by PV modules, resulting in maps reported in GWh·km^{-2}·yr^{-1} for both horizontal and optimally tilted configurations.

The atlas is presented in two complementary forms. First, it shows the intrinsic national PV production surface, independent of deployment constraints. Second, the same continuous annual AC yield surfaces are intersected with the suitable-land masks derived for the three planning configurations examined in Section 4.2, namely the current on-grid scenario, the proposed North–South grid-connection scenario, and the off-grid (infrastructure-independent) scenario. In this way, the atlas provides not only a description of Algeria's spatial PV resource, but also a scenario-dependent representation of the fraction of that resource that remains deployable under different infrastructure assumptions. Fig. 9 presents these results for horizontal PV systems, while Fig. 10 presents the corresponding results for optimally tilted PV systems; in both figures, panel (a) shows the national unconstrained atlas, whereas panels (b), (c), and (d) correspond to the current on-grid, North–South interconnection, and off-grid configurations, respectively.

The national unconstrained atlas (Fig. 9a and Fig. 10a) reveals a clear and coherent north-to-south gradient in annual AC energy yield across Algeria. In both configurations, the Saharan domain exhibits the highest land-normalized production potential, whereas the northern coastal and highland belt shows lower values due to weaker solar input and more frequent atmospheric attenuation. Horizontal PV yields span approximately 202–281 GWh·km^{-2}·yr^{-1}, while optimally tilted systems reach approximately 243–309 GWh·km^{-2}·yr^{-1}, confirming that tilt

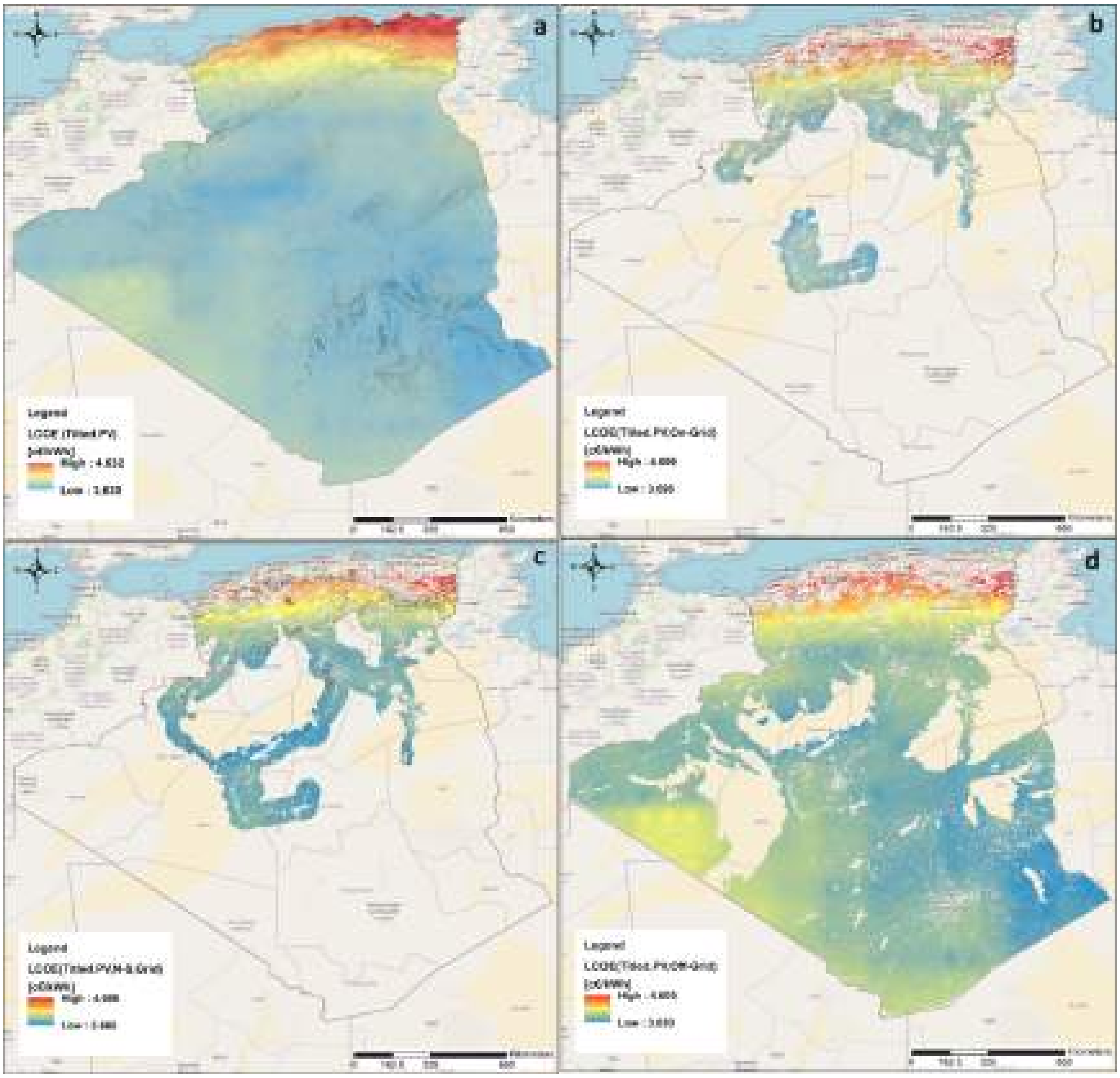

Fig. 13. Spatial distribution of the levelized cost of electricity (LCOE) for utility-scale optimally tilted photovoltaic systems in Algeria under different planning configurations: (a) national unconstrained LCOE surface; (b) LCOE distribution under the current on-grid scenario; (c) LCOE distribution under the proposed North–South grid-connection scenario; and (d) LCOE distribution under the off-grid (infrastructure-independent) scenario. Units: c€/kWh.

optimization systematically increases annual energy density across most of the country while preserving the same broad spatial hierarchy. This pattern indicates that Algeria's strongest PV resource base is concentrated in the south, where higher irradiance and more persistent clear-sky conditions outweigh the adverse effect of elevated operating temperatures.

When the atlas is conditioned by the current on-grid scenario (Fig. 9b and Fig. 10b), the energy-yield surface becomes spatially restricted to land that is simultaneously productive and retained by the existing grid-accessibility logic. As a result, the national resource field contracts into corridor-like structures and isolated southern clusters. The main implication is that the current transmission system captures only a limited share of Algeria's highest-yield land. In other words, many Saharan areas with strong PV productivity do not disappear because of poor resource quality, but because they remain weakly connectable under the present grid configuration. The on-grid atlas therefore represents not the country's full solar-production potential, but the subset that is currently most compatible with existing network access.

Under the proposed North–South interconnection scenario (Fig. 9c and Fig. 10c), this limitation is visibly relaxed. High-yield southern zones become more spatially continuous, and the accessible energy landscape extends farther into the Sahara than in the current on-grid case. The key effect is not only an increase in retained area, but an increase in the amount of high-energy–density land that becomes realistically integrable within a national transmission framework. This is particularly important in the Algerian context, where demand is concentrated in the north while the most favorable PV production zones are located in the south. The North–South scenario therefore operates as a spatial bridge between demand geography and production geography, transforming a larger share of intrinsically productive Saharan land into technically and strategically connectable deployment space.

The off-grid or infrastructure-independent configuration (Fig. 9d and Fig. 10d) most closely reflects the intrinsic national atlas, except where environmental and land-eligibility exclusions remove unsuitable terrain. These panels provide an upper-bound view of the deployable solar resource when grid-distance, road-access, and settlement-proximity constraints are removed from the analysis. Their comparison with the two grid-linked scenarios is particularly informative because it distinguishes zones that are resource-rich but infrastructure-limited from zones that remain constrained even in the absence of grid dependence. This benchmark role is valuable for planning, as it helps identify where future transmission or access investments would produce the largest

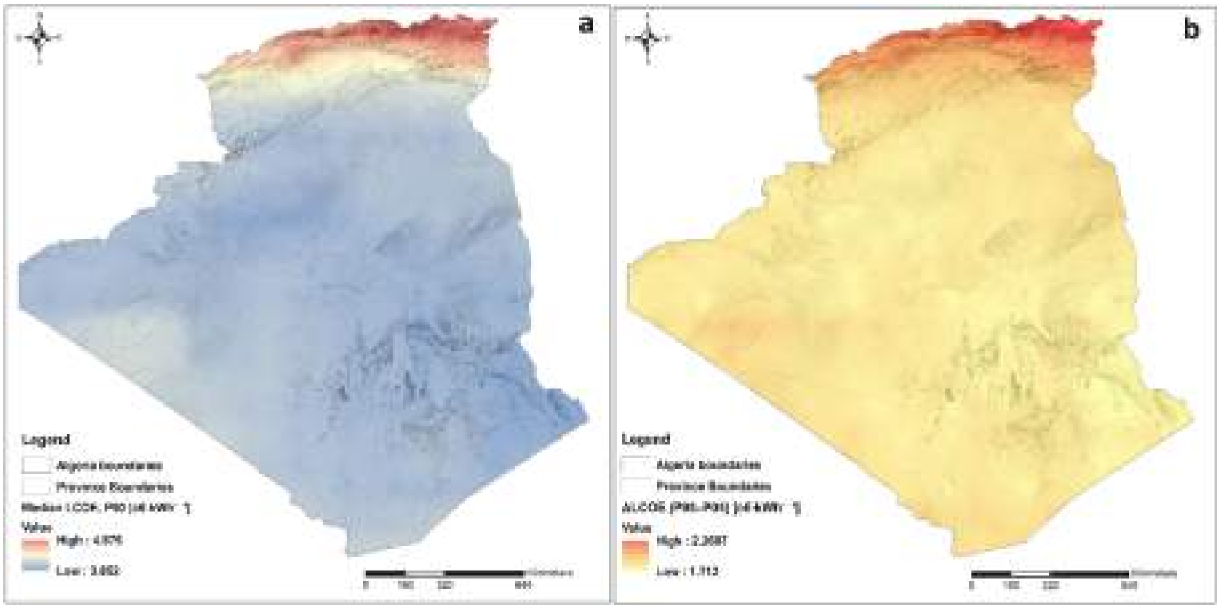

Fig. 14. Monte Carlo uncertainty analysis of spatial LCOE for utility-scale PV systems in Algeria: **(a)** median LCOE surface, **LCOE(P50)**; (b) uncertainty-width surface, ΔLCOE = P95 − P05. Units: c€/kWh.

marginal gains by unlocking already high-performing PV land.

A further consistent result across Figs. 9 and 10 is that the difference between horizontal and optimally tilted systems is primarily one of energy magnitude rather than spatial ordering. The same regional pattern remains visible in both figures, but the tilted configuration systematically shifts the yield surface upward across all planning configurations. Thus, tilt optimization does not fundamentally alter the geography of PV opportunity in Algeria; rather, it strengthens the production advantage of already favorable regions, particularly in the Saharan south. This reinforces the strategic relevance of these areas for both grid-connected expansion and infrastructure-independent deployment pathways.

Overall, the PV Atlas provides a quantitative link between resource assessment, land suitability, and deployment strategy. It shows that the areas identified as favorable for PV development, especially in southern Algeria, are not only suitable in relative multicriteria terms but also deliver the highest annual AC energy densities per unit land area. At the same time, by conditioning the atlas on different infrastructure configurations, the analysis makes explicit how much of this intrinsic production potential is currently accessible, how much could be unlocked through North–South transmission reinforcement, and how much remains available under infrastructure-independent deployment concepts.

Building on the titled PV Atlas results, the next step is to translate the spatial AC energy yields into a planning-relevant metric: the total land footprint required to supply specified electricity-demand targets.

Accordingly, the tilted-atlas production surface is converted into concrete deployment footprints under three benchmarks: EU-27 (2,697 TWh), Italy (306.1 TWh), and Algeria (93.7 TWh). The results indicate that these demand levels could theoretically be met using spatially concentrated deployment footprints, with the In Salah region consistently emerging as a prime candidate due to its high AC yield, extensive undeveloped land, and strategic position relative to major transmission corridors (Fig. 11).

Importantly, the areas reported here represent the total project footprint, assuming that, within each 1 km^2 of project land, only 33.75%, [86,87] is effectively occupied by PV modules (Land, km^2), i.e., the gross land envelope required to accommodate utility-scale PV deployment, including row spacing, internal access roads, electrical equipment areas (inverters/transformers), and other balance-of-plant needs. Under the In Salah benchmark, the estimated footprints required to satisfy the annual electricity demand are 19,969 km^2 for EU-27, 2,266 km^2 for Italy, and 694 km^2 for Algeria. Overall, these results highlight the exceptional role of Algeria's Saharan regions, particularly In Salah, as a strategic hub for large-scale solar production. Beyond satisfying national demand, the analysis also illustrates the longer-term potential for southern Algeria to contribute to regional clean-energy transitions, including prospective supply to Mediterranean and European markets, contingent on grid reinforcement, north–south transmission development, and cross-border integration pathways.

3.4. Economic and environmental assessment

This section evaluates whether the priority PV zones identified by the suitability analysis can deliver electricity at competitive generation costs and quantifies the associated climate benefit in terms of avoided CO_2 emissions. Together, the LCOE and CO_2 layers provide an integrated feasibility check that links spatial resource quality, infrastructure conditions, and decarbonization relevance.

3.4.1. LCOE mapping and cost-competitiveness

The scenario-conditioned LCOE maps were obtained by overlaying the continuous national LCOE surfaces with the suitable-land masks derived for each planning configuration. The resulting spatial patterns indicate that utility-scale PV in Algeria is economically competitive at the national scale, while exhibiting clear regional gradients primarily governed by PV productivity. Fig. 12 presents the LCOE surfaces for horizontal PV systems, whereas Fig. 13 presents the corresponding results for optimally tilted systems, each shown for the unconstrained national case and for the three planning configurations considered in this study.

The unconstrained LCOE surfaces (Fig. 12a and Fig. 13a) reveal a pronounced north-to-south gradient, with higher values in the northern belt and lower values across the Saharan south. This pattern reflects weaker solar input and stronger atmospheric attenuation in the north, versus higher irradiance and more persistent clear-sky conditions in southern Algeria. Under the adopted assumptions, horizontal PV spans approximately 3.99–5.55c€/kWh, whereas the optimally tilted configuration improves cost performance to approximately 3.63–4.63c€/kWh, confirming that tilt optimization lowers plant-gate generation cost through higher annual electricity yield.

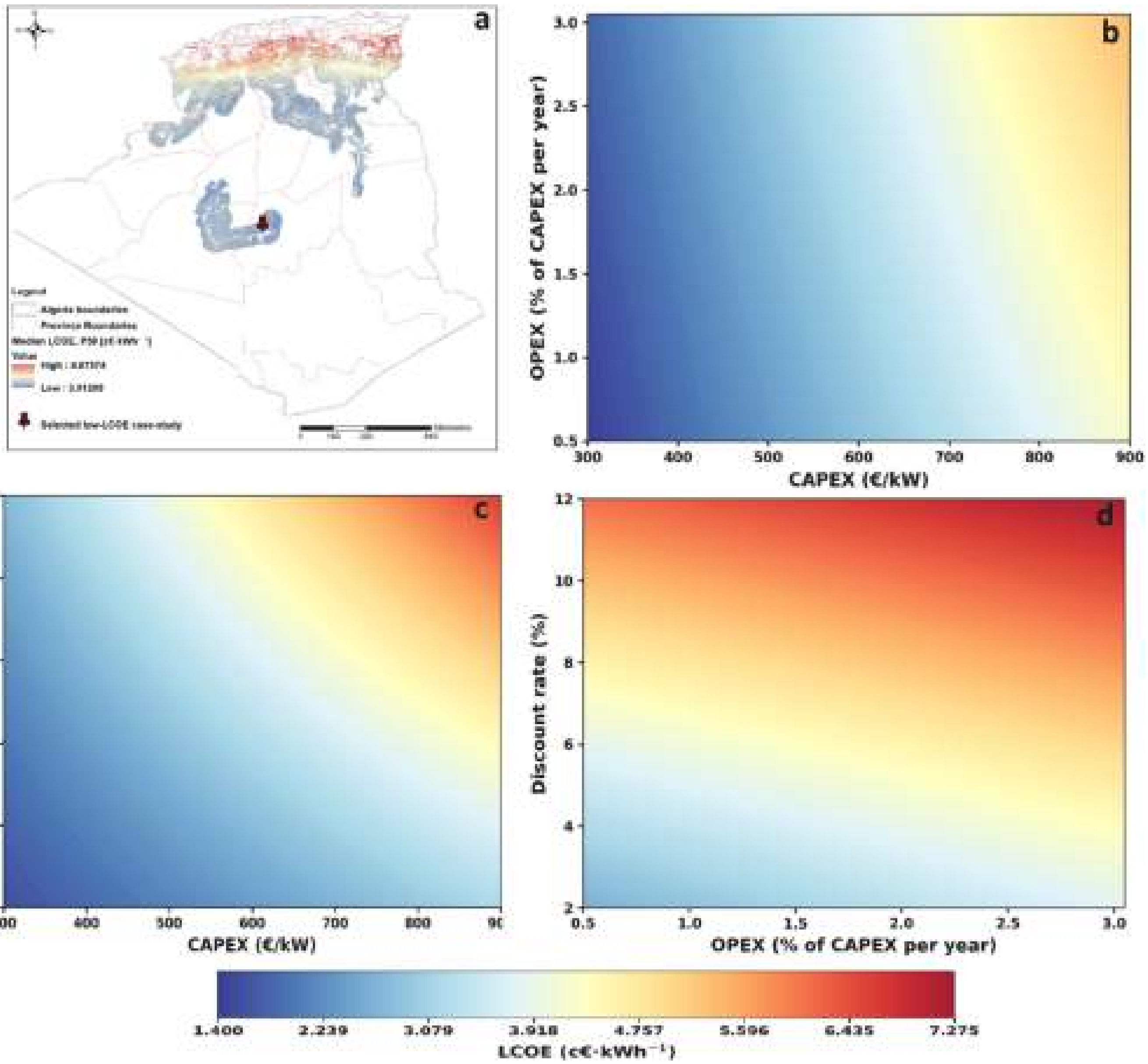

Fig. 15. Site-specific economic sensitivity analysis for a representative low-LCOE grid-connected PV location in Algeria: (a) selected case-study site shown on the median LCOE(P50) surface; (b) LCOE sensitivity to OPEX and discount rate; (c) LCOE sensitivity to CAPEX and OPEX; and (d) LCOE sensitivity to CAPEX and discount rate. Units: c€/kWh.

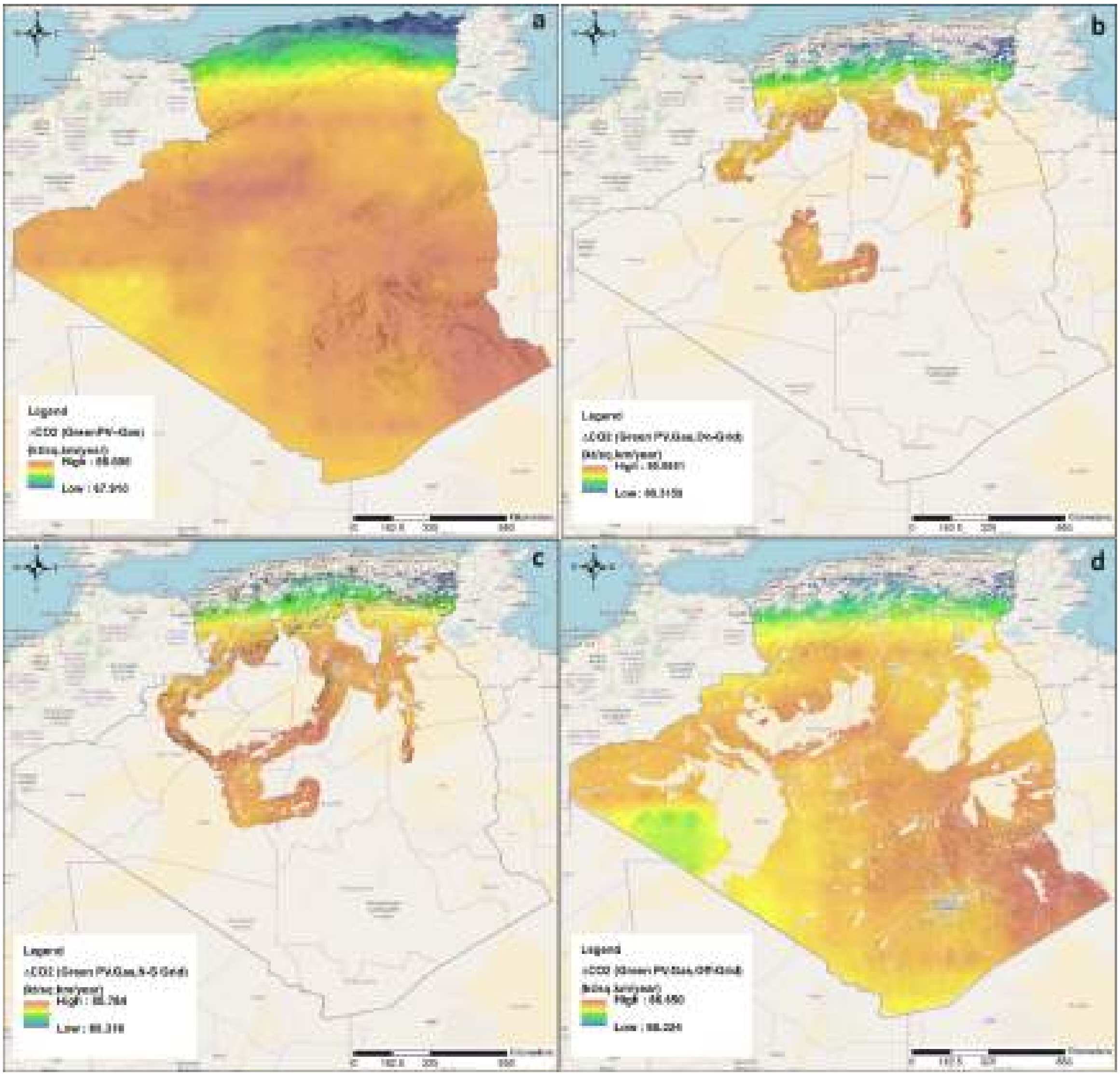

Fig. 16. Spatial distribution of indicative avoided CO_2 emissions for utility-scale optimally tilted photovoltaic systems in Algeria under different planning configurations: (a) national unconstrained mitigation surface; (b) avoided-CO_2 distribution under the current on-grid scenario; (c) avoided-CO_2 distribution under the proposed North–South grid-connection scenario; and (d) avoided-CO_2 distribution under the off-grid (infrastructure-independent) scenario. Units: kt $CO_2 \cdot km^{-2} \cdot yr^{-1}$.

When conditioned by the current on-grid scenario (Fig. 12b and Fig. 13b), the low-cost resource becomes restricted to the subset of productive land that is compatible with the existing grid-accessibility framework. The North–South interconnection scenario (Fig. 12c and Fig. 13c) relaxes this limitation by extending connectable low-LCOE corridors farther into the Saharan south, thereby improving the practical accessibility of Algeria's most competitive PV land. The off-grid scenario (Fig. 12d and Fig. 13d) most closely reproduces the intrinsic national cost gradient and thus provides an upper-bound view of Algeria's underlying cost competitiveness when infrastructure constraints are removed. Across all scenarios, tilt optimization improves LCOE without materially changing the broad spatial ranking of opportunity.

To assess robustness beyond the deterministic surfaces, a Monte Carlo uncertainty analysis was performed for the spatial LCOE evaluation of utility-scale PV systems. For each eligible grid cell, 10,000 simulations were carried out by propagating uncertainty in the principal techno-economic inputs. These inputs included CAPEX (±15%), OPEX (±25%), WACC (5–11%, mode 7%), degradation rate (0.1–0.6% yr^{-1}; most likely 0.25% yr^{-1}), and annual yield perturbation represented by a truncated normal distribution (σ = 7%). Based on these simulations, P05, P50, and P95 statistics were derived, from which the median LCOE map, LCOE(P50), and the uncertainty-width map, ΔLCOE = P95 − P05, were generated (Fig. 14a,b).

For a more localized interpretation, a representative low-LCOE grid-connected case-study site was selected from the median Monte Carlo surface (Fig. 15a) and used for a targeted economic sensitivity analysis. At this site, baseline yield was held constant while CAPEX, OPEX, and discount rate were varied over predefined ranges to isolate their individual effects on LCOE (Fig. 15b–d). The resulting LCOE spans approximately 1.4–7.27 c€/kWh, confirming that financing and cost assumptions can substantially alter project competitiveness even at a favorable location. Among the tested parameters, the discount rate and CAPEX exert the strongest influence, while OPEX has a more moderate but still non-negligible effect.

Overall, the economic analysis shows that Algeria offers nationally competitive utility-scale PV generation costs, particularly in the southern high-resource regions. At the same time, the Monte Carlo and local sensitivity results demonstrate that the economic attractiveness of these sites remains conditional on financing terms and capital-cost assumptions. The combined framework therefore links national-scale spatial screening with site-level economic robustness, providing a stronger basis for investment-oriented PV planning.

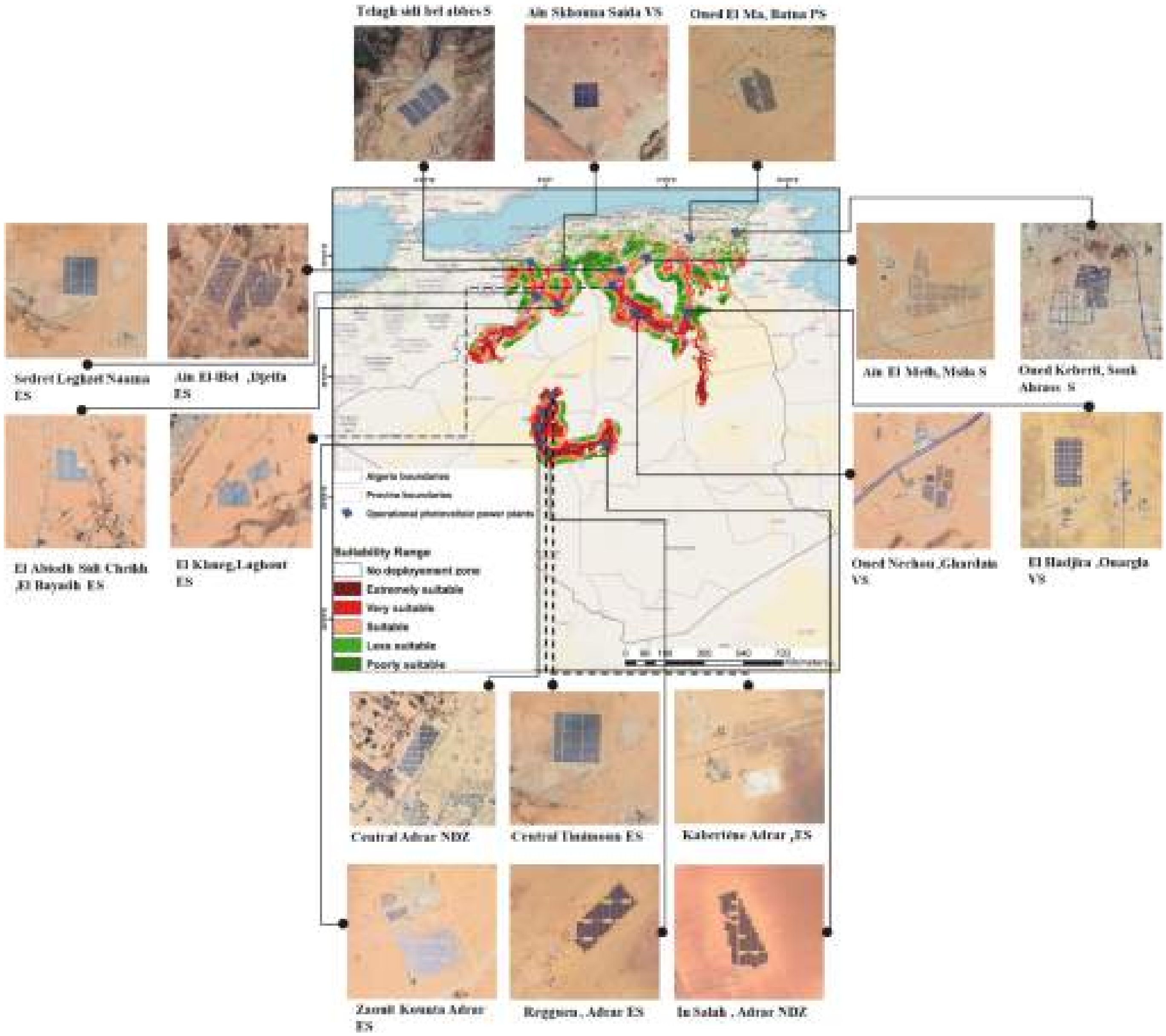

Fig. 17. Validation of the grid-connected photovoltaic suitability mapping using the spatial distribution of operational PV power.

3.4.2. CO_2 mitigation potential and policy relevance

The environmental assessment was derived from the annual AC electricity yield of optimally tilted PV systems, using the methodology described in Section 3.2, and is presented as an indicative avoided CO_2 mitigation intensity under four planning configurations (Fig. 16a–d). The scenario-conditioned avoided-CO_2 maps were obtained by overlaying the continuous mitigation surface derived from the optimally tilted PV yield with the suitable-land masks corresponding to each planning configuration. Because the calculation is directly linked to annual PV output, the spatial mitigation pattern closely follows the underlying production gradient: areas with higher land-normalized electricity yield also exhibit higher avoided-emissions potential per unit area.

The unconstrained map (Fig. 16a) shows the highest mitigation intensities in the southern and southeastern Saharan regions, where PV productivity is strongest, while lower values occur in the northern coastal and highland belt. Under the current on-grid scenario (Fig. 16b), this high-abatement potential becomes restricted to the subset of productive land that remains compatible with the existing grid-accessibility framework. The North–South interconnection scenario (Fig. 16c) relaxes this limitation by extending access to additional high-yield southern areas, thereby increasing the share of land where strong PV output and higher avoided-CO_2 potential can be jointly realized. The off-grid scenario (Fig. 16d) most closely reflects the intrinsic mitigation pattern, apart from the exclusion of non-eligible terrain, and therefore provides an upper-bound view of the spatial decarbonization potential.

Overall, Fig. 16 confirms that the southern regions of Algeria combine stronger PV productivity with higher indicative avoided-CO_2 intensities, reinforcing their strategic relevance for solar deployment. However, these results should be interpreted as indicative spatial mitigation-intensity maps and a screening-level mitigation indicator, rather than a precise estimate of realized emissions reduction. The analysis reflects operational substitution benefits under a fixed displaced-generation baseline and does not constitute a full life-cycle assessment; manufacturing, replacements, civil works, transmission-related effects, curtailment, dispatch interactions, and future changes in grid carbon intensity are not explicitly modeled.

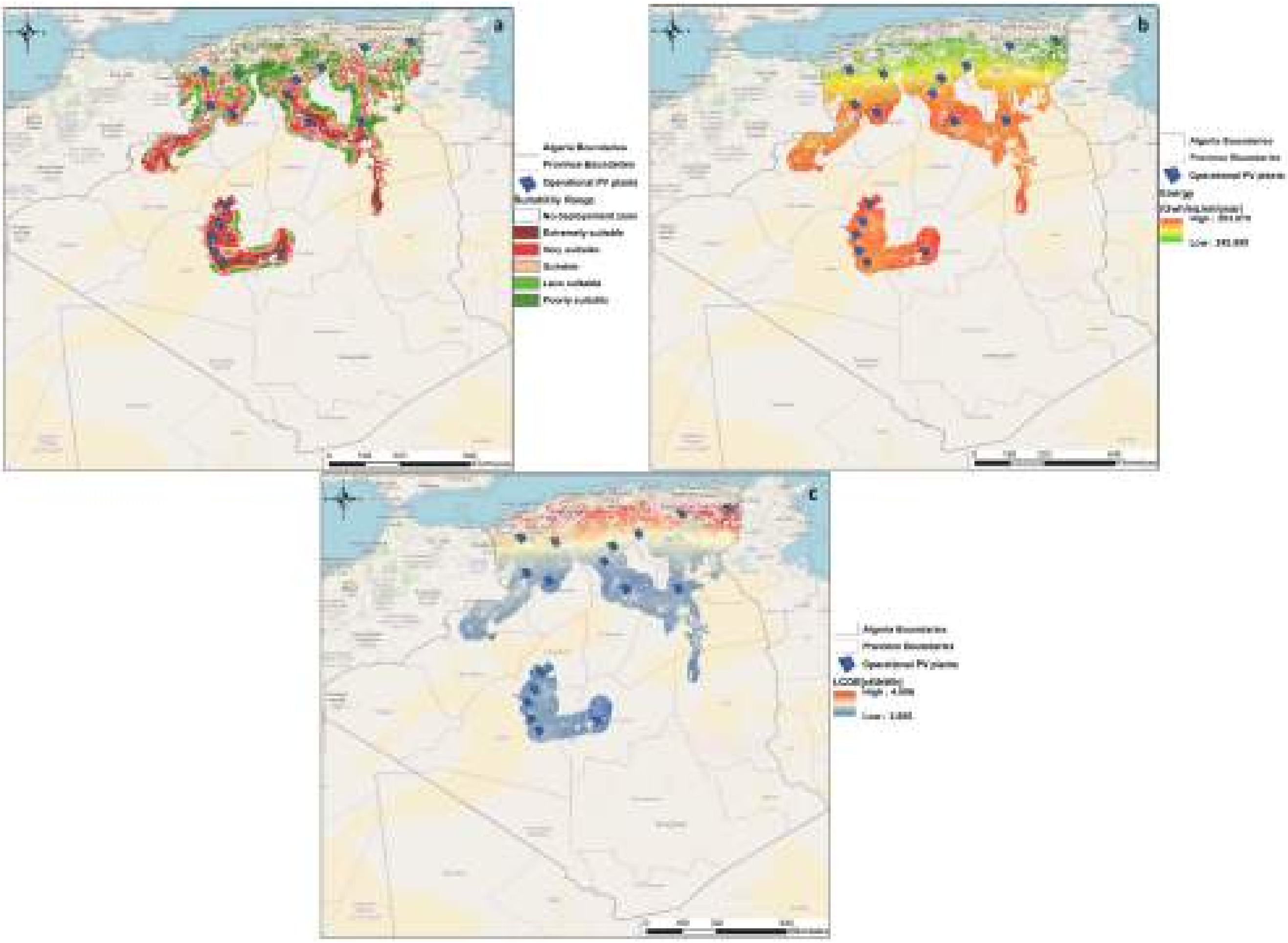

Fig. 18. Joint validation of the photovoltaic suitability mapping using operational PV plant locations overlaid on (a) suitability classes, (b) PV atlas AC energy potential, and (c) LCOE spatial distribution.

4. Discussion and validation

The suitability mapping results were qualitatively validated by comparing the spatial distribution of existing operational, utility-scale, grid-connected photovoltaic power plants with the identified suitability classes. As illustrated in Fig. 17, most installed PV plants are located within areas classified as very suitable or extremely suitable and are directly connected to the national high-voltage power grid. This strong spatial correspondence supports the reliability of the proposed suitability framework and indicates that the selected criteria and weighting schemes capture the main techno-environmental and infrastructural constraints governing real-world PV deployment.

Notably, large installations such as Central Adrar and In Salah are situated within intrinsically extremely suitable zones; however, these sites fall inside areas excluded by the restricted suitability mask adopted in this study, which imposes a minimum buffer distance of 1 km from residential and agricultural regions for utility-scale PV development. Conversely, other operational plants, such as Oued El Ma (Batna), are located within poorly suitable classes, primarily due to lower global solar irradiation and reduced sunshine duration. These observations are further supported by Fig. 18, where the PV atlas AC energy yield for tilted systems and the estimated LCOE distribution consistently align with the grid-connected suitability results. The agreement between suitability mapping, energy potential, economic performance, and actual plant locations confirms the robustness of the proposed framework and supports its applicability for guiding future large-scale photovoltaic planning and deployment.

The spatial screening of Algeria's planned PV portfolio (Table 4; Fig. 19) provides both a practical validation of the proposed framework and a useful diagnostic of planning consistency. The planned pipeline totals approximately 2 GW across 15 utility-scale PV projects. Quantitatively, 8 of the 15 projects (53.3%), representing 1.06 GW (53.0%) of the planned capacity, fall within the high-suitability classes (ES-VS), while 12 projects (80.0%), corresponding to 1.62 GW (81.0%), are located in suitable or better classes (S to ES). This indicates that the planned portfolio is broadly aligned with the favorable zones identified by the framework, although 2 projects (13.3%; 300 MW) remain in low-suitability areas and 1 project (6.7%; 80 MW) falls within a no-development zone.

When the planned sites are compared against the utility-scale suitability classes, PV Atlas AC yield, and the corresponding LCOE surface, a clear techno-economic pattern emerges. Projects in the ES-VS classes generally coincide with the highest modeled energy yields and the lowest LCOE values. This is observed for projects in Bechar (Abadla, Kenadsa), Ghardaia (Guerrara), Touggourt, El M'Ghair (Tendia), Biskra (Leghrous, Khenguet Sidi Nadji), and Ouled Djellal, where the three indicators converge toward favorable high-resource, high-suitability, and low-cost conditions. By contrast, projects in the S and LS classes show comparatively lower PV Atlas yields and/or higher LCOE values. Representative examples include Batna (Ouled Fadel), which has one of the lowest yields in the portfolio (about 262.7 GWh km^{-2} yr^{-1}) and a relatively high LCOE (about 4.28 cEUR/kWh), as well as Bordj Bou Arreridj (El Euch), Tiaret (K'sar Chellala), and M'sila (Batmete), which also exhibit comparatively higher LCOE values. Although these locations

Table 4
Comparison of planned utility-scale photovoltaic projects with atlas-derived suitability class, annual PV yield, and LCOE.

Province – municipality	Land area (ha)	Installed capacity (MW)	Suitability range	Atlas PV (GWh/ km^2/year)	LCOE [c€/ kWh]
Bechar – Abadla	160	80	**ES**	**296.26**	**3.79**
Bechar – Kenadsa	240	120	**ES**	**294.91**	**3.80**
M'sila – Batmete	440	220	**LS**	278.11	4.04
Bordj Bou Arréridj – El Euch	160	80	**S**	269.15	4.18
Batna – Ouled Fadel	160	80	**LS**	262.71	4.28
Laghouat – Ghetiet Sidi Saad	400	200	**S**	**284.97**	**3.94**
Ghardaia – Guerrara	160	80	**VS**	**297.74**	**3.77**
Tiaret – K'sar Chellala	160	80	**S**	275.31	4.08
El Oued – Dour El Maa Nakhla	400	200	**S**	**294.61**	**3.81**
El Oued – Taleb Larbi	160	80	NDZ	**292.96**	**3.83**
Touggourt – Touggourt	300	150	**ES**	**297.28**	**3.77**
El M'Ghair – Tendia	400	200	**ES**	**292.29**	**3.84**
Biskra – Leghrous	400	200	VS	**285.36**	**3.93**
Biskra – Khenguet Sidi Nadji	300	150	VS	**283.71**	**3.96**
Ouled Djellal	160	80	VS	**287.05**	**3.915**

Note: ES = Excellent suitable; VS = Very suitable; S = Suitable; LS = Low suitable; NDZ = Non-developable zone.

are not unsuitable in absolute terms, they offer less techno-economic headroom than the best Saharan clusters and therefore imply a higher opportunity cost when the objective is to maximize electricity output per unit land and investment.

A particularly informative case is El Oued-Taleb Larbi, which is classified as NDZ under the soil-type constraint because it overlaps dune and mobile-sand units. Notably, its PV Atlas yield (about 293.0 GWh km^{-2} yr^{-1}) and LCOE (about 3.83 cEUR/kWh) are otherwise fully consistent with highly favorable Saharan conditions. This contrast shows that resource and cost layers alone may be overly optimistic in geomorphologically dynamic desert environments. It also underlines the value of explicitly accounting for mobile sands in order to avoid siting assets in areas exposed to elevated construction and operational risks, including reduced foundation stability, access-road maintenance needs, windblown sand accumulation, and accelerated soiling.

Overall, most planned projects are broadly aligned with the favorable classes identified by the atlas, while the observed deviations highlight the importance of integrating additional physical constraints into project screening. In practical terms, allocating large capacities to lower-performing zones may reduce annual electricity output per installed MW, increase the cost per delivered kWh, and intensify land-use and grid-integration requirements for the same energy contribution. By contrast, prioritizing the high-suitability and high-yield clusters identified by the framework would improve generation efficiency, strengthen cost competitiveness, and increase avoided emissions per unit investment. The joint interpretation of suitability class, PV Atlas AC yield, and LCOE therefore confirms the practical relevance of the proposed framework as a screening and decision-support tool for guiding future PV deployment in Algeria toward locations where technical performance, economic viability, and environmental benefit are jointly optimized.

5. Limitations and future work

This study provides a national-scale, high-resolution (100 m) PV siting and feasibility framework; however, several limitations should be acknowledged. First, land-use/land-cover (LULC) uncertainty remains a key source of spatial error at national scale. The LULC layer derived from Sentinel-based products may contain classification errors, temporal mismatch, and limited representation of fast-changing land uses, especially across a large and heterogeneous territory such as Algeria. While the analysis applies exclusion masks and cross-layer consistency checks, local discrepancies may persist and could affect site eligibility and suitability ranks in specific areas. Second, some environmental and geomorphological constraints are represented through available proxy layers; higher-fidelity local datasets and ground-validated inventories would improve operational screening in Saharan contexts. Third, although the framework includes spatially explicit discounted LCOE and connection/access cost adders, the economic assessment remains screening-level. In particular, for clusters located far from existing transmission and road infrastructure, the current LCOE does not fully internalize the cost and feasibility of new grid corridors and road construction (including routing constraints, permitting, and right-of-way), which could materially change delivered costs for remote projects.

Future work will focus on improving input fidelity and feasibility realism through more targeted, implementation-oriented analyses. As a first step, a regional follow-up study will examine the highest-suitability zones identified in the national screening. This will allow finer verification of land-use/land-cover (LULC) and other local constraints using higher-resolution datasets and, where feasible, targeted ground-truthing. Such an approach is more tractable and more accurate than attempting detailed validation across the full national extent. Additional priorities include: (i) refining geomorphological operability screening (e.g., dunes/moving sands dynamics) using dedicated desert-surface datasets and, where possible, time-varying indicators; (ii) integrating explicit infrastructure expansion costs by modelling candidate transmission and road corridors, and incorporating corridor CAPEX/OPEX into delivered LCOE for remote clusters.

6. Conclusion

This study presented a comprehensive and integrated spatial framework for photovoltaic (PV) deployment planning in Algeria, combining multi-criteria suitability analysis, grid-connection scenarios, PV atlas–based energy assessment, economic evaluation, and environmental impact analysis. By jointly considering on-grid and off-grid configurations, utility-scale and small-scale PV systems, and both horizontal and optimally tilted module configurations, the proposed methodology provides a robust and versatile decision-support tool for large-scale solar energy planning.

The suitability mapping results highlight the strong influence of grid accessibility, land-use constraints, topography, and environmental exclusion criteria on optimal PV site selection. The proposed grid-connected scenario significantly expands high-suitability areas compared to purely off-grid configurations, demonstrating the critical role of transmission infrastructure in enabling cost-effective large-scale PV deployment. Sensitivity analysis further confirms that while weighting schemes affect the relative extent of suitability classes, the spatial patterns of the most favorable zones remain stable, underscoring the robustness of the adopted criteria selection and weighting strategy.

The PV atlas analysis, based on spatially resolved AC energy yields derived from the Sandia performance model, reveals a pronounced north–south gradient in photovoltaic energy potential, with southern regions exhibiting the highest production levels for both horizontal and tilted systems. When coupled with the economic assessment, the results show a clear spatial coherence between high-energy-yield zones and low

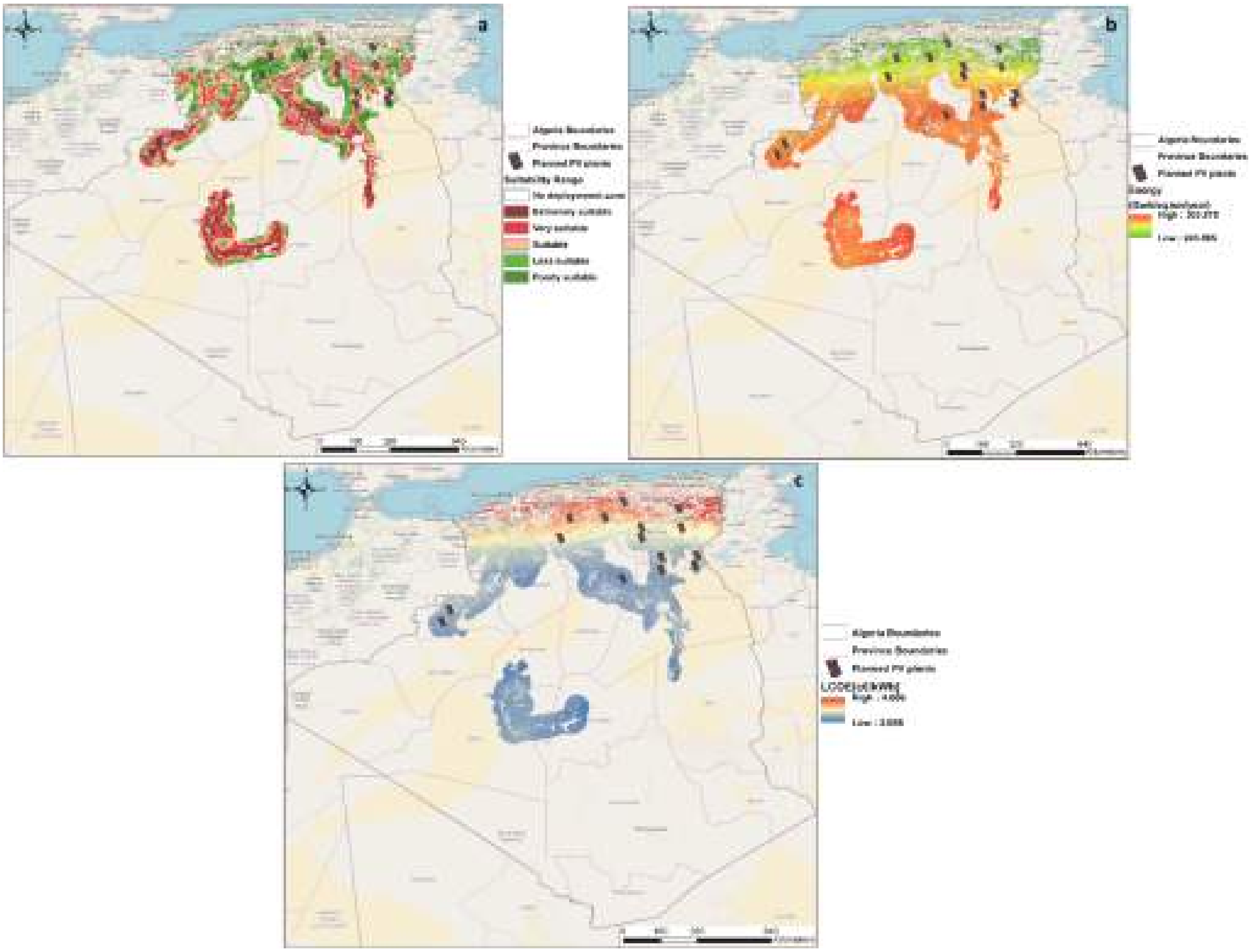

Fig. 19. Evaluation of planned photovoltaic power plant siting relative to (a) suitability classes, (b) PV atlas AC energy potential, and (c) LCOE spatial distribution.

LCOE values, confirming that regions with superior solar resources also offer the most competitive electricity generation costs. Under the adopted assumptions, optimally tilted PV systems achieve LCOE values in the range of approximately 3.63–4.63 c€/kWh, reinforcing the strong cost competitiveness of PV deployment in Algeria.

Importantly, the integration of Monte Carlo uncertainty analysis and site-specific sensitivity assessment provides additional insight into the robustness of these economic results. While the deterministic and median LCOE surfaces preserve the favorable spatial ranking of southern high-resource regions, the sensitivity analysis indicates that LCOE values can vary substantially under different economic conditions. At a representative low-LCOE site, the LCOE spans a wider range of approximately 1.4–7.27 c€/kWh when variations in CAPEX, OPEX, discount rate, degradation rate, and energy yield are considered. This highlights that, although Algeria's PV resource base provides a strong structural advantage, the economic attractiveness of projects remains dependent on financing conditions and cost assumptions, emphasizing the importance of incorporating uncertainty-aware approaches in investment-oriented planning.

The environmental assessment demonstrates that large-scale PV deployment can deliver substantial CO_2 emission reductions, particularly when displacing gas-based electricity generation. The spatial distribution of avoided emissions closely mirrors the PV energy potential and economic performance, further supporting the integrated nature of the approach. Validation against the spatial distribution of operational PV power plants confirms that existing installations predominantly coincide with highly suitable zones, while the assessment of planned PV projects reveals opportunities to improve future siting decisions by avoiding marginal or poorly suitable areas.

Finally, the land-requirement analysis shows that regional electricity demand scenarios for Algeria, Italy, and the EU-27 could be satisfied using realistically constrained land areas, even under conservative assumptions regarding effective PV surface coverage. These findings emphasize the strategic importance of Algeria's Saharan regions—particularly areas such as In Salah—as key locations for large-scale solar deployment with potential relevance beyond national boundaries.

Overall, this work provides a holistic, scalable, and policy-relevant framework that bridges spatial planning, energy modeling, economics, and environmental assessment. The proposed approach can support evidence-based decision-making, guide sustainable PV investment strategies, and contribute meaningfully to the clean energy transition at national and regional scales. Future research may extend this framework by incorporating detailed infrastructure expansion costs, dynamic grid constraints, and sector-coupling options to further enhance long-term planning and deployment strategies.

Declaration of generative AI and AI-assisted technologies in the writing process

During the preparation of this manuscript, the authors used ChatGPT only as a language editing tool, for grammar checking and occasional improvement of sentence clarity. All content was subsequently reviewed and revised by the authors, who accept full responsibility for the final text of the publication.

CRediT authorship contribution statement

Mawloud Guermoui: Visualization, Writing – original draft, Validation, Software, Resources, Methodology, Investigation, Formal analysis, Conceptualization. **Abdelfetah Belaid:** Resources, Methodology, Formal analysis, Data curation. **Abdelkader Riche:** Software, Formal analysis, Data curation. **Farid Melgani:** Writing – review & editing, Validation, Supervision, Resources, Project administration, Investigation, Funding acquisition, Formal analysis, Conceptualization.

Declaration of competing interest

The authors declare that they have no known competing financial interests or personal relationships that could have appeared to influence the work reported in this paper.

Acknowledgement

This work is supported by the EU Horizon Europe MSCA Postdoctoral Fellowship RESSAIG, Grant Agreement No. 101197884. Funded by the European Union. Views and opinions expressed are however those of the author(s) only and do not necessarily reflect those of the European Union or The European Research Executive Agency. Neither the European Union nor the granting authority can be held responsible for them.

Appendix A

This appendix reports the fuzzy analytic hierarchy process (FAHP) calculations used to derive the expert-based criteria weights adopted in the suitability analysis. Expert judgments were collected through pairwise comparisons using a Saaty-9 linguistic scale represented by triangular fuzzy numbers (TFNs). The resulting TFN pairwise comparison matrix for the selected criteria set is provided in Table A1.

Criteria priorities were computed using the fuzzy geometric mean approach, followed by fuzzy normalization and centroid (center-of-area) defuzzification to obtain a single crisp weight for each criterion. The final weights were then normalized to sum to one, as reported in Table A2. The results indicate that resource-related drivers dominate the weighting structure, with GHI receiving the highest importance, followed by grid proximity and sunshine duration, while atmospheric and terrain-related modifiers (Linke turbidity, albedo, aspect) receive lower weights.

For the sensitivity tests, an equal-weight scheme was included in which all criteria were assigned identical importance (uniform weights). In addition, a literature-based weighting scheme was compiled from prior PV siting studies [22–26,33,36,37,43,61,67–69,88,89]. In this literature scheme, Linke turbidity was not considered (hence no assigned weight), while cloudy days was included as a proxy for atmospheric conditions. In the present study, cloudy days was not used because it is largely redundant with the sunshine-duration indicator. The resulting weights for the three schemes are reported in Table A2.

Table A1
Expert-based triangular fuzzy pairwise comparison matrix for the criteria used in the FAHP weighting.

	Global horizontal irradiance	Distance to power grid	Sunshine duration	Distance to roads	Ambient air temperature	Distance land use	Slope	Surface albedo	Linke turbidity	Terrain aspect
Global Horizontal Irradiance	(1,1,1)	(1,2,3)	(2,3,4)	(2,3,4)	(2,3,4)	(3,4,5)	(4,5,6)	(7,8,9)	(9,9,9)	(9,9,9)
Distance to Power Grid	(1/3,1/2,1)	(1,1,1)	(1,1,1)	(1,1,1)	(1,2,3)	(1,2,3)	(1,2,3)	(3,4,5)	(4,5,6)	(7,8,9)
Sunshine Duration	(1/4,1/3,1/2)	(1,1,1)	(1,1,1)	(1,1,1)	(1,1,1)	(1,2,3)	(1,2,3)	(2,3,4)	(3,4,5)	(5,6,7)
Distance to Roads	(1/4,1/3,1/2)	(1,1,1)	(1,1,1)	(1,1,1)	(1,1,1)	(1,2,3)	(1,2,3)	(2,3,4)	(3,4,5)	(5,6,7)
Ambient Air Temperature	(1/4,1/3,1/2)	(1/3,1/2,1)	(1,1,1)	(1,1,1)	(1,1,1)	(1,1,1)	(1,2,3)	(1,2,3)	(2,3,4)	(3,4,5)
Distance Land Use	(1/5,1/4,1/3)	(1/3,1/2,1)	(1/3,1/2,1)	(1/3,1/2,1)	(1,1,1)	(1,1,1)	(1,1,1)	(1,2,3)	(1,2,3)	(3,4,5)
Slope	(1/6,1/5,1/4)	(1/3,1/2,1)	(1/3,1/2,1)	(1/3,1/2,1)	(1/3,1/2,1)	(1,1,1)	(1,1,1)	(1,2,3)	(1,2,3)	(2,3,4)
Surface Albedo	(1/9,1/8,1/7)	(1/5,1/4,1/3)	(1/4,1/3,1/2)	(1/4,1/3,1/2)	(1/3,1/2,1)	(1/3,1/2,1)	(1/3,1/2,1)	(1,1,1)	(1,1,1)	(1,2,3)
Linke Turbidity	(1/9,1/9,1/9)	(1/6,1/5,1/4)	(1/5,1/4,1/3)	(1/5,1/4,1/3)	(1/4,1/3,1/2)	(1/3,1/2,1)	(1/3,1/2,1)	(1,1,1)	(1,1,1)	(1,2,3)
Terrain Aspect	(1/9,1/9,1/9)	(1/9,1/8,1/7)	(1/7,1/6,1/5)	(1/7,1/6,1/5)	(1/5,1/4,1/3)	(1/5,1/4,1/3)	(1/4,1/3,1/2)	(1/3,1/2,1)	(1/3,1/2,1)	(1,1,1)

Table A2
Criterion weighting schemes used in the GIS–MCDA analysis: FAHP-derived normalized weights and alternative equal- and literature-based weights.

Criteria	Expert weights from fuzzy-AHP	Equal weights Scenario	Literature weights scenario
Global Horizontal Irradiance	0.2858	0.1	0.243954
Distance to Power Grid	0.1451	0.1	0.136741
Sunshine Duration	0.1180	0.1	0.054003
Distance to Roads	0.1180	0.1	0.071272
Ambient Air Temperature	0.0941	0.1	0.085783
Distance Land Use	0.0747	0.1	0.078722

(*continued on next page*)

Table A2 (*continued*)

Criteria	Expert weights from fuzzy-AHP	Equal weights Scenario	Literature weights scenario
Slope	0.0682	0.1	0.092762
Surface Albedo	0.0404	0.1	0.060349
Linke Turbidity	0.0343	0.1	–
Terrain Aspect	0.0214	0.1	0.113632
Cloudy Days	–	–	0.113632

Appendix B

Appendix B presents supplementary utility-scale PV suitability maps under equal and literature-based weighting schemes, evaluated with/without the soil exclusion mask. Results are shown for the existing grid (Fig. B1) and the proposed north–south grid-connection scenario (Fig. B2).

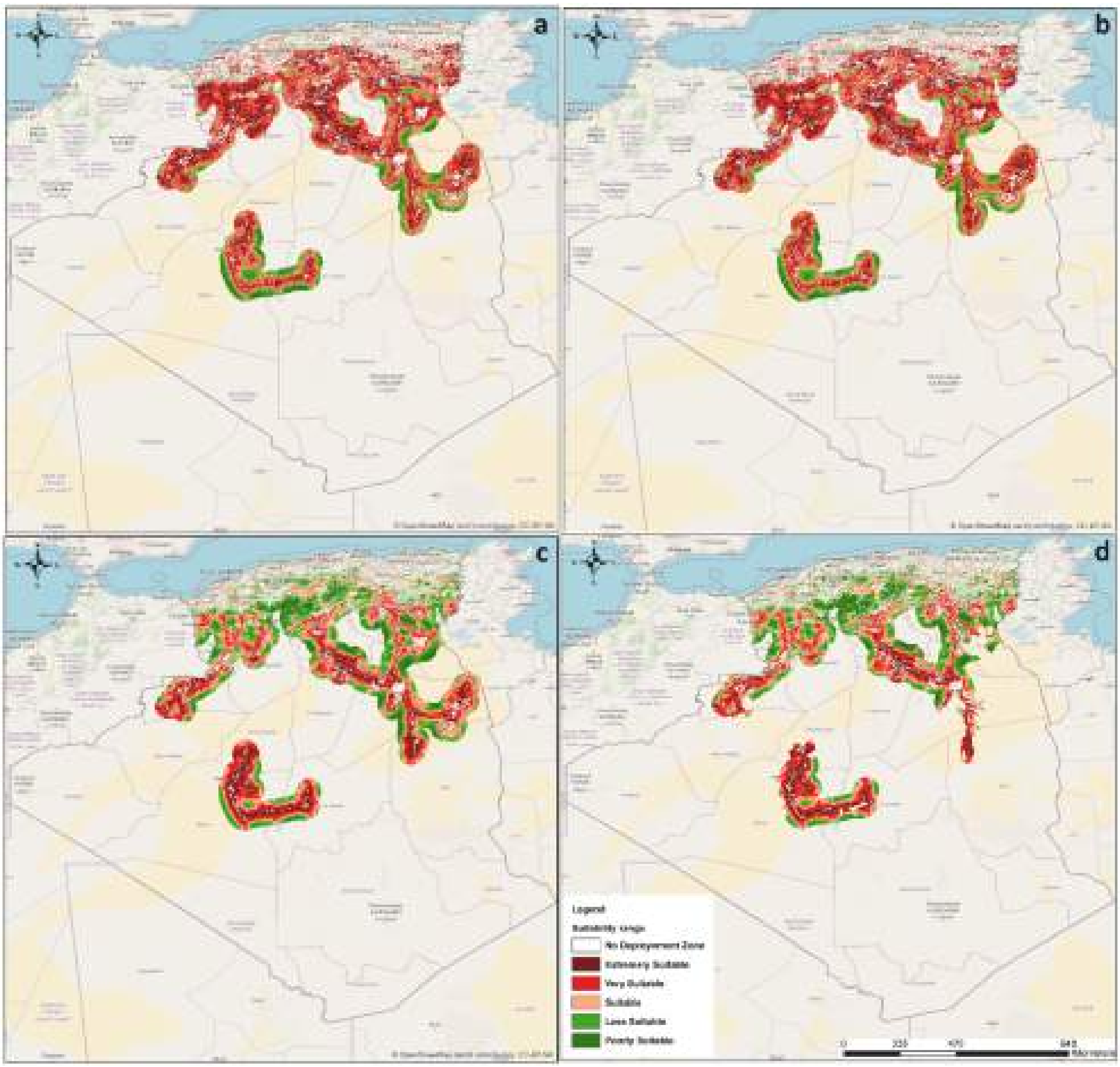

Fig. B1. Utility-scale PV suitability maps under alternative weighting schemes and soil-mask configurations: (a) equal weights without soil mask, (b) equal weights with soil mask, (c) literature-based weights without soil mask, and (d) literature-based weights with soil mask.

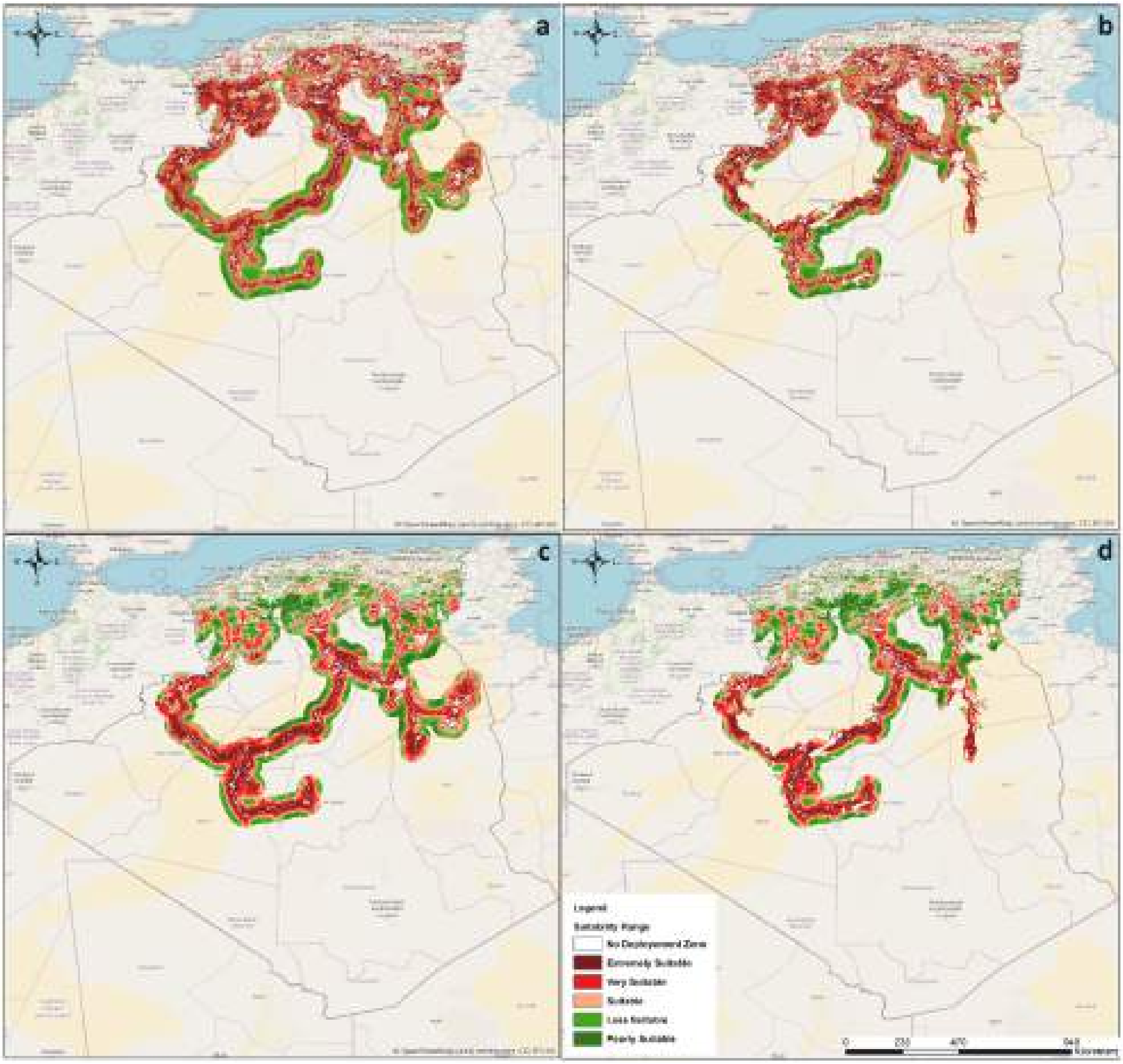

Fig. B2. Utility-scale PV suitability under the proposed north–south grid-connection scenario for alternative weighting schemes and soil-mask configurations: (a) equal weights without soil mask, (b) equal weights with soil mask, (c) literature-based weights without soil mask, and (d) literature-based weights with soil mask.

Data availability

All input data used for the analyses are publicly shared on Zenodo (https://zenodo.org/records/18232449). The datasets generated and/or analysed during the current study, including the processed layers and model outputs, will be deposited in the same repository.

References

[1] International Energy Agency (IEA). Global Energy Review 2025. Paris: IEA; 2025. Available from: https://www.iea.org/reports/global-energy-review-2025 (accessed 24 Oct 2025).

[2] International Energy Agency (IEA). World Energy Outlook 2024. Paris: IEA; 2024. Available from: https://www.iea.org/reports/world-energy-outlook-2024 (accessed 24 Oct 2025).

[3] International Energy Agency (IEA). Pathways for the energy mix. In: World Energy Outlook 2023. Paris: IEA; 2023. Available from: https://www.iea.org/reports/world-energy-outlook-2023/pathways-for-the-energy-mix (accessed 24 Oct 2025).

[4] International Energy Agency (IEA). CO_2 emissions. In: Global Energy Review 2025. Paris: IEA; 2025. Available from: https://www.iea.org/reports/global-energy-review-2025/co2-emissions (accessed 24 Oct 2025).

[5] International Energy Agency (IEA). A new era for CCUS. In: CCUS in Clean Energy Transitions. Paris: IEA; 2020. Available from: https://www.iea.org/reports/ccus-in-clean-energy-transitions/a-new-era-for-ccus (accessed 24 Oct 2025).

[6] International Energy Agency (IEA). CCUS projects around the world are reaching new milestones. Commentary. Paris: IEA; 30 Apr 2025. Available from: https://www.iea.org/commentaries/ccus-projects-around-the-world-are-reaching-new-milestones (accessed 24 Oct 2025).

[7] International Renewable Energy Agency. (2025). *Renewable power generation costs in 2024*. IRENA. https://www.irena.org/Publications/2025/Jun/Renewable-Power-Generation-Costs-in-2024 (accessed October 25, 2025).

[8] Zambrano-Asanza S, Quiros-Tortos J, Franco JF. Optimal site selection for photovoltaic power plants using a GIS-based multi-criteria decision making and spatial overlay with electric load. Renew Sustain Energy Rev 2021;143:110853. https://doi.org/10.1016/j.rser.2021.110853.

[9] Al Garni, Hassan Z, Anjali Awasthi. "Solar PV power plants site selection: a review." Advances in renewable energies and power technologies (2018): 57–75. Doi: 10.1016/B978-0-12-812959-3.00002-2.

[10] Sánchez-Lozano JM, Socorro García-Cascales M, Lamata MT. Comparative TOPSIS-ELECTRE TRI methods for optimal sites for photovoltaic solar farms. Case study in Spain. J Clean Prod 2016;127:387–98. https://doi.org/10.1016/j.jclepro.2016.04.005.

[11] Zoghi M, et al. Optimization solar site selection by fuzzy logic model and weighted linear combination method in arid and semi-arid region: a case study Isfahan-IRAN. Renew Sustain Energy Rev 2017;68:986–96. https://doi.org/10.1016/j.rser.2015.07.014.

[12] Doorga, Jay RS, Rughooputh SD, Boojhawon R. Multi-criteria GIS-based modelling technique for identifying potential solar farm sites: a case study in Mauritius. Renew Energy 2019;133:1201–19. https://doi.org/10.1016/j.renene.2018.08.105.

[13] Imam AA, Abusorrah A, Marzband M. Potentials and opportunities of solar PV and wind energy sources in Saudi Arabia: land suitability, techno-socio-economic feasibility, and future variability. Results Eng 2024;21:101785. https://doi.org/10.1016/j.rineng.2024.101785.

[14] Halimi Y, et al. Spatially-optimized photovoltaic site selection in Algeria: Assessing solar potential using high-resolution data, GIS, and multicriteria analysis. Energy Convers Manage 2025;323:119176. https://doi.org/10.1016/j.enconman.2024.119176.

[15] Díaz-Cuevas P, Haddad B, Fernandez-Nunez M. "Energy for the future: Planning and mapping renewable energy. The case of Algeria. Sustain Energy Technol Assess 2021;47:101445.". https://doi.org/10.1016/j.seta.2021.101445.

[16] Wang Y, et al. Locating the suitable large-scale solar farms in China's deserts with environmental considerations. Sci Total Environ 2024;955:176911. https://doi.org/10.1016/j.scitotenv.2024.176911.

[17] Hamad JU, Ahmad M, Zeeshan M. Solar energy resource mapping, site suitability and techno-economic feasibility analysis for utility scale photovoltaic power plants in Afghanistan. Energy Convers Manage 2024;303:118188. https://doi.org/10.1016/j.enconman.2024.118188.

[18] Nafi'shehab Z, Faisal RM, Ahmed SW. Multi-criteria decision making (MCDM) approach for identifying optimal solar farm locations: a multi-technique comparative analysis. Renew Energy 2024;237:121787. https://doi.org/10.1016/j.renene.2024.121787.

[19] Rekik S, El Alimi S. "A gis based mcdm modelling approach for evaluating large-scale solar pv installation in tunisia. Energy Rep 2024;11:580–596.". https://doi.org/10.1016/j.egyr.2023.12.018.

[20] Al-Awadhi T, et al. Solar farms suitability analysis using GIS-Based Analytic Hierarchy Process (AHP) multi-criteria: a case study of Al Duqm–Oman. Renew Energy 2025;241:122295. https://doi.org/10.1016/j.renene.2024.122295.

[21] Elkadeem MR, et al. A spatio-temporal decision-making model for solar, wind, and hybrid systems–a case study of Saudi Arabia. Appl Energy 2025;383:125277. https://doi.org/10.1016/j.apenergy.2025.125277.

[22] Demir A, Ersin Dinçer A, Yılmaz K. A novel procedure for the AHP method for the site selection of solar PV farms. Int J Energy Res 2024;2024(1):5535398. https://doi.org/10.1155/2024/5535398.

[23] Zhao H, Chen Lu, Zhang Y. Optimal site selection for wind-photovoltaic-complemented storage power plants based on geographic information system and grey relational analysis-group criteria importance through inter criteria correlation-interactive and multicriteria decision making: a case study of China. J Storage Mater 2024;92:112148. https://doi.org/10.1016/j.est.2024.112148.

[24] Zhang Y, Zhao Z. A novel hybrid multi-criteria decision-making approach for solar photovoltaic power plant site selection based on the quantity and quality matching of resource-demand. Expert Syst Appl 2025;267:126014. https://doi.org/10.1016/j.eswa.2024.126014.

[25] Farfán IA, et al. Socio-environmental and technical factors assessment of photovoltaic hydrogen production in Antofagasta, Chile. Energy Strategy Rev 2024;53:101373. https://doi.org/10.1016/j.esr.2024.101373.

[26] Saraswat SK, Digalwar AK, Vijay V. Analysis of multi-renewable energy potential sites in India using spatial characteristics: a GIS and hybrid MCDM approach. Process Integr Optim Sustain 2024;8(5):1493–526. https://doi.org/10.1007/s41660-024-00441-3.

[27] Flora FMI. A GIS-based on application of Monte Carlo and multi-criteria decision-making approach for site suitability analysis of solar-hydrogen production: case of Cameroon. Heliyon 2025;11(1). https://doi.org/10.1016/j.heliyon.2024.e41541.

[28] Li X-Y, et al. The promising future of developing large-scale PV solar farms in China: a three-stage framework for site selection. Renew Energy 2024;220:119638. https://doi.org/10.1016/j.renene.2023.119638.

[29] Santana-Sarmiento F, Velázquez-Medina S. A method based on GIS techniques to assess renewable energy self-consumption capacity. A case study. Energy 2024;305:132246. https://doi.org/10.1016/j.energy.2024.132246.

[30] Metegam IFF, et al. Evaluation of on-grid and off-grid solar photovoltaic sites in Cameroon using geographic information systems, fuzzy logic, and multi-criteria analysis. Energy 2025;318:134614. https://doi.org/10.1016/j.energy.2025.134614.

[31] Yilmaz İ, Kocer A, Aksoy E. Site selection for solar power plants using GIS and fuzzy analytic hierarchy process: case study of the western mediterranean region of Turkiye. Renew Energy 2024;237:121799. https://doi.org/10.1016/j.renene.2024.121799.

[32] Xiao S, et al. Land reuse for carbon mitigation: Decarbonization potential of solar photovoltaics in China's open-pit mining areas. Land Use Policy 2025;158:107768. https://doi.org/10.1016/j.landusepol.2025.107768.

[33] Richards D, et al. Sustainable solar energy deployment: a multi-criteria decision-making approach for site suitability and greenhouse gas emission reduction. Environ Sci Pollut Res 2025;32(4):2007–35. https://doi.org/10.1007/s11356-024-35669-6.

[34] Elkadeem MR, Younes A, Mazzeo D, et al. Geospatial-assisted multi-criterion analysis of solar and wind power geographical-technical-economic potential assessment. Appl Energy 2022;322:119532. https://doi.org/10.1016/j.apenergy.2022.119532.

[35] Okazawa Y, Hino K, Asami Y. Photovoltaic power plant installation in the Tokyo metropolitan area, Japan, focusing on land use and regulatory ordinances. Land Use Policy 2025;152:107495. https://doi.org/10.1016/j.landusepol.2025.107495.

[36] Vasudevan V, Gundabattini E, Darius Gnanaraj S. Geographical Information System (GIS)-based solar photovoltaic farm site suitability using multi-criteria approach (MCA) in Southern Tamilnadu, India. J Inst Eng (India): Ser C 2024;105(1):81–99. https://doi.org/10.1007/s40032-023-01001-3.

[37] Li X, Dong X, Ye Y. An interaction model applied to optimize photovoltaic farm location: a case study of China. Appl Energy 2024;356:122421. https://doi.org/10.1016/j.apenergy.2023.122421.

[38] Boube BD, et al. Topic: geospatial evaluation of solar potential for hydrogen production site suitability: GIS-MCDA approach for off-grid and utility or large-scale systems over Niger. Energy Rep 2025;13:2393–416. https://doi.org/10.1016/j.egyr.2025.01.032.

[39] Bawazir RO, Çetin NS, Fadel W. Optimum ground-mounted on-grid connected photovoltaic system. J Clean Prod 2024;447:141294. https://doi.org/10.1016/j.jclepro.2024.141294.

[40] Flora FMI. An MCDM-GIS based site suitability analysis for solar power plant integration in Cameroon: solar hybridization to optimize green electricity and hydrogen production. Int J Hydrogen Energy 2025;106:23–51. https://doi.org/10.1016/j.ijhydene.2025.01.445.

[41] Ali MZ, et al. Assessing solar energy potential and CO_2 reduction through GIS-based spatial analysis for optimal site selection of photovoltaic systems in Jeddah, Saudi Arabia. Remote Sens Appl: Soc Environ 2025;38:101537. https://doi.org/10.1016/j.rsase.2025.101537.

[42] Fan S, et al. Assessment of solar energy resource potential in the western region of Jilin province: a multi-dimensional framework based on availability, stability and concentration. Renew Energy 2025:124422. https://doi.org/10.1016/j.renene.2025.124422.

[43] Sharma T, Sarin A. Multi-criteria decision making for solar site selection in Punjab, India: an evaluation of site suitability using hybrid MCDM techniques towards the goal of sustainable energy development. Results Eng 2025:106288. https://doi.org/10.1016/j.rineng.2025.106288.

[44] Tang L, et al. Optimizing solar photovoltaic plant siting in Liangshan Prefecture, China: a policy-integrated, multi-criteria spatial planning framework. Solar Energy 283 2024:113012. https://doi.org/10.1016/j.solener.2024.113012.

[45] Onuoha H, et al. Integrating GIS and AHP for photovoltaic farm site selection: a case study of Ikorodu, Nigeria. Processes 2025;13(1):164. https://doi.org/10.3390/pr13010164.

[46] Akay SS. Investigating land suitability for PV farm and existing sites using a multi-criteria decision approach in Gaziantep, Türkiye. Appl Sci 2025;15(5):2441. https://doi.org/10.3390/app15052441.

[47] Ashraf HA, et al. Geographic information system and machine learning approach for solar photovoltaic site selection: a case study in Pakistan. Processes 2025;13(4):981. https://doi.org/10.3390/pr13040981.

[48] Shen J, et al. A high spatial resolution suitability layers to support feasible power plant site selection in China. Sci Data 2025;12(1):608. https://doi.org/10.1038/s41597-025-04937-6.

[49] Lamien MHY, Farzaneh H. Integrated land use land cover-energy modeling framework for solar energy planning in the future expansion areas; the case of Luxor city Region, Egypt. Energy Convers Manage: X 2025;25:100874. https://doi.org/10.1016/j.ecmx.2025.100874.

[50] Yang H, et al. Mapping development potential and priority zones for utility-scale photovoltaic on the Qinghai-Tibet Plateau. Renew Energy 2024;237:121546. https://doi.org/10.1016/j.renene.2024.121546.

[51] Demir A, Dincer AE, Yılmaz K. A novel method for the site selection of large-scale PV farms by using AHP and GIS: a case study in İzmir, Türkiye. Solar Energy 2023;259:235–45. https://doi.org/10.1016/j.solener.2023.05.031.

[52] Aliabadi Y, et al. Sustainable solar energy potential using GIS-PVSOL: an integrated technical, economic, environmental and social analysis in Qazvin, Iran. Results Eng 2025:107088. https://doi.org/10.1016/j.rineng.2025.107088.

[53] Shi F, et al. Site selection strategy for photovoltaic power plants construction on gangue hills: an integrated method based on GIS and AHP-TOPSIS. Energy Strategy Rev 2025;59:101722. https://doi.org/10.1016/j.esr.2025.101722.

[54] Khazael SM, et al. Enhancing solar PV suitability mapping in the Middle East using an optimized deep learning framework. Alexandria Eng J 2025;129:553–71. https://doi.org/10.1016/j.aej.2025.06.059.

[55] Bertsiou MM, et al. Optimal site selection for wind and solar parks in Karpathos Island using a GIS-MCDM model. ISPRS Int J Geo Inf 2025;14(3):125. https://doi.org/10.3390/ijgi14030125.

[56] Dinçer AE, Demir A, Yılmaz K. Enhanced objectivity of AHP for more reliable solar farm site selection. Energy Sci Eng 2025;13(5):2315–29. https://doi.org/10.1002/ese3.70027.

[57] Guermoui M, et al. An analysis of case studies for advancing photovoltaic power forecasting through multi-scale fusion techniques. Sci Rep 2024;14(1):6653. https://doi.org/10.1038/s41598-024-57398-z.

[58] **U.S. EIA.** *Country Analysis Brief: Algeria.* Washington, DC: U.S. Energy Information Administration; 2025; p. (renewables target 15 GW by 2035). Accessed 25 Oct 2025.

[59] Enerdata. "Sonelgaz launches a 700 km transmission project to link Algeria's power grids." Daily Energy News; 2023. Accessed 25 Oct 2025.

[60] Reuters. “Algeria’s oil and gas firms sign MoU with Eni for electricity supply, Sonatrach says.” 31 Jul 2024. Accessed 25 Oct 2025.

[61] Bouraiou A, et al. Status of renewable energy potential and utilization in Algeria. J Clean Prod 2020;246:119011. https://doi.org/10.1016/j.jclepro.2019.119011.

[62] Eichhammer W. Étude Évaluation et Analyse du Marché du Power-to-X et des Opportunités d'Investissement en Algérie. Atelier de Clôture, 18 Avril 2024. Karlsruhe: Fraunhofer Institute for Systems and Innovation Research ISI. 2024.

[63] Nasser M, Hassan H. Egyptian green hydrogen Atlas based on available wind/solar energies: power, hydrogen production, cost, and CO_2 mitigation maps. Int J Hydrogen Energy 2024;50:487–501. https://doi.org/10.1016/j.ijhydene.2023.09.127.

[64] Aly A, Jensen SS, Pedersen AB. Solar power potential of Tanzania: Identifying CSP and PV hot spots through a GIS multicriteria decision making analysis. Renew Energy 2017;113:159–75. https://doi.org/10.1016/j.renene.2017.05.077.

[65] Giamalaki M, Tsoutsos T. Sustainable siting of solar power installations in Mediterranean using a GIS/AHP approach. Renew Energy 2019;141:64–75. https://doi.org/10.1016/j.renene.2019.03.100.

[66] Pereira JMC, Duckstein L. A multiple criteria decision-making approach to GIS-based land suitability evaluation. Int J Geogr Inf Sci 1993;7(5):407–24. https://doi.org/10.1080/02693799308901971.

[67] Schroedter-Homscheidt M, Oumbe A, Benedetti A, Morcrette JJ. Aerosols for concentrating solar electricity production forecasts: requirement quantification and ECMWF/MACC aerosol forecast assessment. Bull Am Meteorol Soc 2013;94(6):903–14. https://doi.org/10.1175/BAMS-D-11-00259.1.

[68] Guermoui M, et al. Enhancing direct Normal solar Irradiation forecasting for heliostat field applications through a novel hybrid model. Energy Convers Manage 2024;304:118189. https://doi.org/10.1016/j.enconman.2024.118189.

[69] Elboshy BH, et al. A suitability mapping for the PV solar farms in Egypt based on GIS-AHP to optimize multi-criteria feasibility. Ain Shams Eng J 2022;13(3):101618. https://doi.org/10.1016/j.asej.2021.10.013.

[70] Almasad A, et al. Site suitability analysis for implementing solar PV power plants using GIS and fuzzy MCDM based approach. Solar Energy 2023;249:642–50. https://doi.org/10.1016/j.solener.2022.11.046.

[71] Rios R, Duarte S. Selection of ideal sites for the development of large-scale solar photovoltaic projects through analytical hierarchical process–geographic information systems (AHP-GIS) in Peru. Renew Sustain Energy Rev 2021;149:111310. https://doi.org/10.1016/j.rser.2021.111310.

[72] Kereush D, Perovych I. Determining criteria for optimal site selection for solar power plants. Geomat Landmanagement Landsc 2017;4:39–54. https://doi.org/10.15576/GLL/2017.4.39.

[73] Ali S, et al. GIS based site suitability assessment for wind and solar farms in Songkhla, Thailand. Renew Energy 2019;132:1360–72. https://doi.org/10.1016/j.renene.2018.09.035.

[74] Merrouni AA, et al. Large scale PV sites selection by combining GIS and Analytical Hierarchy Process. Case study: Eastern Morocco. Renew Energy 2018;119:863–73. https://doi.org/10.1016/j.renene.2017.10.044.

[75] Garni AL, Hassan Z, Awasthi A. Solar PV power plants site selection: a review. Adv Renew Energies Power Technol 2018:57–75. https://doi.org/10.1016/B978-0-12-812959-3.00002-2.

[76] Wang Q, Poh KL. A survey of integrated decision analysis in energy and environmental modeling. Energy 2014;77:691–702. https://doi.org/10.1016/j.energy.2014.09.060.

[77] Mardani A, et al. Sustainable and renewable energy: an overview of the application of multiple criteria decision making techniques and approaches. Sustainability 2015;7(10):13947–84. https://doi.org/10.3390/su71013947.

[78] Aydin NY, Kentel E, Duzgun HS. GIS-based site selection methodology for hybrid renewable energy systems: a case study from western Turkey. Energy Convers Manage 2013;70:90–106. https://doi.org/10.1016/j.enconman.2013.02.004.

[79] Ghasemi G, et al. Theoretical and technical potential evaluation of solar power generation in Iran. Renew Energy 2019;138:1250–61. https://doi.org/10.1016/j.renene.2019.02.068.

[80] Rekik S, Souheil EA. Optimal wind-solar site selection using a GIS-AHP based approach: a case of Tunisia. Energy Convers Manage: X 2023;18:100355. https://doi.org/10.1016/j.ecmx.2023.100355.

[81] Saaty TL. A scaling method for priorities in hierarchical structures. J Math Psychol 1977;15(3):234–81. https://doi.org/10.1016/0022-2496(77)90033-5.

[82] Laarhoven V, Peter JM, Pedrycz W. A fuzzy extension of Saaty’s priority theory. Fuzzy Sets Syst11 1983;(1-3):229–41. https://doi.org/10.1016/S0165-0114(83)80082-7.

[83] Chang D-Y. Applications of the extent analysis method on fuzzy AHP. Eur J Oper Res 1996;95(3):649–55. https://doi.org/10.1016/0377-2217(95)00300-2.

[84] Perez R, et al. Modeling daylight availability and irradiance components from direct and global irradiance. Solar Energy 1990;44(5):271–89. https://doi.org/10.1016/0038-092X(90)90055-H.

[85] Peng J, et al. Validation of the Sandia model with indoor and outdoor measurements for semi-transparent amorphous silicon PV modules. Renew Energy 2015;80:316–23. https://doi.org/10.1016/j.renene.2015.02.017.

[86] Milbrandt A, Mann M. *Potential for hydrogen production from key renewable resources in the United States* (Technical Report No. NREL/TP-640-41134). National Renewable Energy Laboratory. Doi: 10.2172/899141. 2007.

[87] Bolinger M, Bolinger G. Land requirements for utility-scale PV: an empirical update on power and energy density. IEEE J Photovoltaics 2022;12(2):589–94. https://doi.org/10.1109/JPHOTOV.2021.3136805.

[88] Rekik S, Souheil EA. A GIS based MCDM modelling approach for evaluating large-scale solar PV installation in Tunisia. Energy Rep 2024;11:580–96. https://doi.org/10.1016/j.egyr.2023.12.018.

[89] Saraswat SK, Digalwar AK, Vijay V. Analysis of multi-renewable energy potential sites in India using spatial characteristics: a GIS and Hybrid MCDM approach. Process Integr Optim Sustain 2024;8(5):1493–526. https://doi.org/10.1007/s41660-024-00441-3.